NATIONAL ADVISORY COMMITTEE FOR AERONAUTICS

TECHNICAL NOTE 3491

EXPERIMENTAL INVESTIGATION OF ECCENTRICITY RATIO, FRICTION, AND OIL FLOW OF LONG AND SHORT JOURNAL BEARINGS WITH LOAD-NUMBER CHARTS

By G. B. DuBois, F. W. Ocvirk, and R. L. Wehe

Cornell University

Washington

September 1955

U

NATIONAL ADVISORY COMMITTEE FOR AERONAUTICS

TECHNICAL NOTE 3491

EXPERIMENTAL INVESTIGATION OF ECCENTRICITY RATIO, FRICTION, AND OIL FLOW OF LONG AND SHORT JOURNAL BEARINGS WITH LOAD-NUMBER CHARTS

By G. B. DuBois, F. W. Ocvirk, and R. L. Wehe

SUMMARY

The performances of plain bearings under steady central loading are compared and summarized by single-line curves covering the range of length-diameter ratios both above and below 1. Experimental data on eccentricity ratio, friction, and oil flow for length-diameter ratios of 1, $1\frac{1}{2}$, and 2 are shown for comparison with earlier data for length-diameter ratios of 1/4, 1/2, and 1. The combined data provide charts of plain-bearing performance which cover the practical range of length-diameter ratio.

The load number l/C_n in the form $p/\mu N'(c_d/d)^2(d/l)^2$, where C_n is the capacity number, p is the central unit bearing load, μ is the oil viscosity, N' is the journal speed, c_d is the diametral bearing clearance, d is the bearing diameter, and l is the bearing length, is used as the basic variable on which eccentricity, friction, and oil flow rate depend. Charts are presented to show that the eccentricity-ratio data fall nearly on a single line for both long and short bearings if the $(d/l)^2$ term in the load number is taken as unity for bearings of l/d greater than 1; in effect, the load number for long bearings becomes the reciprocal of the Sommerfeld number $1/S$. Friction and oil flow rate, however, are shown to depend on the load number without this modification, for both long and short bearings.

Plots of friction data in terms of friction ratio F/F_o are presented to focus attention on the difference between journal friction and bearing friction. Experimental journal-friction data from other sources are included.

Analytical curves by Sommerfeld, Cameron, and Wood and the short-bearing approximation are shown for comparison with the experimental data for eccentricity ratio and friction. Curves resulting from the integration of Sommerfeld's pressure-distribution function for an extent of 180° of the pressure film are also shown.

INTRODUCTION

In an earlier report (ref. 1), the analytical curves of the short-bearing approximation were found to be in useful agreement with experimental data on eccentricity, friction, and oil flow for centrally loaded plain bearings with values of l/d of 1/4, 1/2, and 1. A few early experiments with bearings of l/d of 2 indicated that it was necessary, with regard to eccentricity, to limit the usefulness of the curves to bearings of l/d not exceeding 1. For this reason, a conclusion was drawn that further testing on bearings of l/d between 1 and 2 was necessary to cover the range of bearing configurations used in practice.

The new experimental data in the present report were obtained from tests conducted in the Machine Design Laboratories at Cornell University, Ithaca, New York, as a part of a bearing-research investigation conducted under the sponsorship and with the financial aid of the National Advisory Committee for Aeronautics. Experimental data on bearings of $1\frac{3}{8}$-inch diameter with l/d ratios of 3/4, 1, $1\frac{1}{2}$, and 2 are reported herein and correlated with existing data for values of l/d of 1/4, 1/2, and 1. In the long-bearing tests, loads up to 1,700 pounds or 875 pounds per square inch were used at speeds up to 7,000 rpm with SAE 10 oil and with clearances ranging from 0.0018 to 0.0038 inch. The data are combined in charts covering the range of values of l/d in common use. The integrations for the Sommerfeld π case are given in the appendix which was prepared by Professor Wehe.

Analytical Background

Analytical solutions by Cameron and Wood (ref. 2) giving points locating curves for l/d ratios of 1/4, 1/2, 1, and infinity are available. Sommerfeld (ref. 3) provides an analytical solution for bearings of infinite l/d. The short-bearing approximation applies best to short bearings and is useful in the range of values of l/d up to 1. Thus, no analytical solutions for l/d in the neighborhood of 2 are available. This experimental investigation was initiated to provide experimental data, particularly on eccentricity, using bearings of $l/d = 1$, $1\frac{1}{2}$, and 2. A short bearing of $l/d = 3/4$ was also included in order that

a parallel investigation on the misalining characteristics of bearings (ref. 4) could be conducted using the same test bearings and journals. The equipment and technique used in the experimentation were similar to those reported in reference 1 for the short bearings.

In his solution for bearings of infinite length, Sommerfeld showed that the basic nondimensional grouping of bearing variables on which eccentricity and friction depend is the Sommerfeld number

$$S = \frac{\mu N'}{p}\left(\frac{d}{c_d}\right)^2 \tag{1}$$

For finite short bearings, the short-bearing approximation yields single-line curves of eccentricity ratio and friction using the capacity number C_n as the basic variable:

$$C_n = \frac{\mu N'}{p}\left(\frac{d}{c_d}\right)^2\left(\frac{l}{d}\right)^2 \tag{2}$$

It may be seen that the variables of equations (1) and (2) are different by the factor $(l/d)^2$.

Load Number

The reciprocal of the capacity number, or load number $1/C_n$, is used in figures 1 to 4. The load number, which is the reciprocal form of the basic variable, is chosen in order to expand the interesting high-load region and to show the variation of eccentricity, friction, and oil flow rate in direct proportion to the central load.

The experimental data on eccentricity, friction, and oil flow rate in figures 1 to 4 show the extent to which the Sommerfeld number and load number reduce data to nearly single line charts for bearings of l/d from 1/4 to 2. The influence of the $(l/d)^2$ term in this regard is shown. Charts of experimental data from reference 1 for bearings of l/d = 1/4, 1/2, and 1 are reproduced in figures 1(b), 2(b), and 4(b) for comparison with charts of data reported herein in figures 1(a) to 4(a) on bearings of l/d = 1, $1\frac{1}{2}$, and 2.

Friction Ratio

In figure 2, the ratio of the friction torque measured on the bearing to the analytical Petroff friction at no load, the friction

ratio F/F_o, is used as a basic variable (ref. 1). This is believed to be more convenient to use than the coefficient of friction f based on load and focuses attention to the quantities on which friction directly depends. A similar ratio, the power-loss ratio j, is used by Wilcock and Rosenblatt (ref. 5). The friction ratio is shown analytically to depend on the load number by the short-bearing approximation.

It is generally recognized that the friction torque on the journal is greater than the friction torque on the bearing by the amount of the couple caused by the lateral displacement of the journal in the bearing. The line of action of the load and its supporting reaction are separated by this displacement to form a couple. The difference in friction is considerable under certain conditions and can be shown on a single curve in figure 3 by plotting the couple friction ratio $\Delta F/F_o(d/l)^2$ against the load number.

Oil Flow Factor

The oil flow rate from the test bearing is represented in figure 4 by a single-line curve obtained by the use of the oil flow factor q, which is the ratio of the experimental flow rate to the analytical end leakage rate of the converging wedge portion of the oil film. This is plotted against a modification of the load number called the inlet-oil-pressure number $1/C_{p_o}$, in which the inlet oil supply pressure is substituted for the unit bearing pressure in the load number. This method of plotting oil flow rate is the same as that used in the earlier report covering values of l/d less than 1 (ref. 1) except that the reciprocal form of the number is used in this report.

SYMBOLS

Dimensional quantities:

c_d diametral bearing clearance, in.

c_r radial bearing clearance, $c_d/2$, in.

d bearing diameter, in.

e eccentricity for central loading, in.

e_h lateral displacement of journal, in.

e_v vertical displacement of journal, in.

F_b friction force on stationary bearing surface, lb

F_j friction force on rotating journal surface, lb

F_o Petroff friction force at no load and zero eccentricity, $2\pi^2\mu N'\ell d(d/c_d)$, lb

ℓ bearing length, in.

N journal speed, rpm

N' journal speed, rps

p_{film} local fluid film pressure, lb/sq in.

p applied central unit bearing load on projected area, lb/sq in.

p_c capsule pressure of load, lb/sq in.

p_o inlet oil pressure, lb/sq in.

p_s pressure at $\theta = 0$ and π in Sommerfeld solution, lb/sq in.

P applied central bearing load, lb

P_X, P_Y components of central load parallel and normal to line of bearing and journal centers, lb

Q experimental total rate of oil flow from bearing, cu in./sec

r bearing radius, in.

t_4, t_9 temperature at stations 4 and 9, respectively, ^oF

U surface speed of journal, in./sec

μ oil viscosity, $\frac{\text{centipoise}}{6.9 \times 10^6}$ or reyns

θ angular variable giving local film pressure, deg

ϕ attitude angle, angle between load line and line of centers of bearing and journal, deg

Nondimensional quantities:

c_d/d	clearance ratio
C_n	capacity number, $\frac{\mu N'}{p}\left(\frac{d}{c_d}\right)^2\left(\frac{l}{d}\right)^2$
C_{p_o}	inlet-pressure capacity number, $\frac{\mu N'}{p_o}\left(\frac{d}{c_d}\right)^2\left(\frac{l}{d}\right)^2$
$1/C_n$	load number for values of l/d less than 1
$1/C_{p_o}$	inlet-oil-pressure number
f	coefficient of friction, F/P
F/F_o	friction ratio
F_b/F_o	bearing friction ratio
F_j/F_o	journal friction ratio
$\Delta F/F_o$	couple friction ratio
l/d	length-diameter ratio
n	eccentricity ratio or attitude for central loading, e/c_r
n_h	horizontal component of eccentricity ratio, e_h/c_r
n_v	vertical component of eccentricity ratio, e_v/c_r
q	oil flow factor, $\frac{Q}{\pi d l c_d (N'/2) n}$
S	Sommerfeld number, $\frac{\mu N'}{p}\left(\frac{d}{c_d}\right)^2$
$1/S$	load number for values of l/d greater than 1
x,y	coordinates
Z	viscosity, centipoise

APPARATUS

The bearing-testing machine used in these experiments is illustrated in figures 5 to 8 and is the same as that described in reference 1. The manner in which the test elements were supported and loaded is shown in figures 5 and 6. Figure 7 shows the mechanical system for measuring journal displacements, and figure 8 gives the locations of the thermocouples used to determine bearing temperatures.

Test Bearing and Journals

A single bronze bearing and five steel shafts of $1\frac{3}{8}$-inch nominal diameter were used in the configuration shown in figure 5. Each of the shafts represented a given length-diameter ratio and a given clearance as listed below:

Shaft	l/d	Average diametral clearance, c_d, in.	Clearance ratio, c_d/d, in./in.
6A	2	0.00252	0.00183
6B	2	.00376	.00273
6C	$1\frac{1}{2}$	.00196	.00142
6D	1	.00183	.00133
6E	$\frac{3}{4}$	.00258	.00187

These test elements were also used in the misalinement experiments as reported in reference 4. SAE 10 oil was used as the test lubricant and was fed to the test bearing at a pressure of 40 to 160 pounds per square inch through a 1/8-inch-diameter oil hole located opposite the central load. The oil was preheated to 140° F near the pump, but the temperature of the oil was measured as it entered the bearing because of small heat losses in the oil lines.

The test shafts were driven by a high-speed, direct-current, variable-speed aircraft motor having a speed range of 1,000 to 10,000 rpm.

Loading Apparatus

As shown in figure 6, the central load was applied hydraulically by a pressure capsule and was transmitted to the bearing through an oil-pressurized spherical seat. The oil flow through the spherical seat floats the bearing giving it freedom to rotate and displace on the application of central load. The line of action of the load passes through the center of the spherical seat, which is located accurately at the center of the bearing.

Displacement Measurements

The coordinate displacements of the journal ends relative to the bearing were measured by the mechanical arrangement illustrated in figure 7 in which horizontal and vertical motions are transmitted by bronze riders on levers through vertical rods to four 0.0001-inch dial indicators. This is the same system reported in reference 1 except that the levers were modified to give a 2:1 magnification of the displacements to improve the accuracy in reading the dials. A duplicate set of rods is used for temperature compensation.

Friction Torquemeter

Friction torque was measured by the hydraulic torquemeter shown in figure 6. The torquemeter consists of two 1/2-inch pistons which are connected to the mast extending from the test bearing so that the piston forces oppose each other. A flow of light oil is forced into the space at the head of each piston and is discharged through ports partially covered by the pistons. The friction torque of the bearing applies a force to the pistons to cause a slight change in the discharge port area, resulting in a pressure differential on the two pistons to balance the applied force. The pistons are centered in their bores by a pressurizing system of relieved areas, thus eliminating frictional contact.

The difference in pressure on the two pistons is indicated by a mercury manometer and is proportional to the torque on the test bearing. Manometer readings were converted to friction torque by direct calibration under running conditions by applying known increments of moment to the bearing hub by the weights shown in figure 6 and recording the corresponding changes in the manometer readings.

Oil Flow Measurements

As shown in figure 6, a drain hole in the bottom of the machine housing allows the oil flowing from the test bearing to be collected

in a pan which may be removed for weighing. Also shown are the slinger rings and baffles which prevent the mixing of the test-bearing oil with the oil from the support bearings and the spherical seat.

Temperature Measurement

Iron-constantan thermocouples were used to measure bearing temperatures at 14 locations in the bearing hub within 1/16 inch of the bearing surface as shown in figure 8. Thermocouple 9 gave the bearing-hub temperature at a point 2 inches radially from the oil film, and thermocouple 16 was used to determine the temperature of the incoming oil at the oil inlet to the test bearing.

TEST PROCEDURE

For the five shafts, two series of experiments were conducted at a number of constant speeds and inlet oil pressures. Displacement experiments, in which eccentricity was measured, were made on all shafts. Friction and oil flow experiments were made separately from the displacement tests because of the necessity of disconnecting the bronze riders which were a source of unwanted friction. Measurements of friction and oil flow were made on the longer bearings of $\frac{l}{d} = 1\frac{1}{2}$ and 2.

Displacement Experiments

Variations in displacement were obtained by varying the central load at constant speed. It was found that by operating under constant speed the variations in bearing temperature were small. A nearly constant temperature of the apparatus at thermal equilibrium assured a minimum thermal effect in the measurements. Before the data were taken, the test elements and the measuring apparatus were brought to equilibrium temperature by running them at constant speed and central load for a period of 20 to 30 minutes.

At the end of the warmup period, the net central load and the inlet oil pressure were reduced to zero so that the indicator dials could be set to a datum position representing zero displacement of the journal relative to the bearing. An inlet oil pressure was then applied and held constant. Displacement data as read from the four dials were then recorded for various increments of central load. The load was increased in four to eight increments and then decreased in the same increments to permit averaging of data. The following data were recorded: Journal displacements, capsule pressure of central load, bearing temperatures at

critical locations, inlet oil pressure, speed, direction of rotation, inlet oil temperature, room temperature, and oil temperature after the heater. The same procedure was followed for the opposite direction of rotation so that the data could be averaged for the two rotations. As shown in table I, constant-speed runs at approximately 500, 1,200, 2,500, and 5,000 rpm were conducted for each of the five test shafts to determine the effects of l/d and clearance on the bearing characteristics. The maximum applied central load in the tests was 1,713 pounds on shaft 6C and the maximum unit load on projected area was 874 psi on shaft 6D. The maximum bearing temperature recorded was 198° F at 7,000 rpm for shaft 6D.

Friction and Oil Flow Experiments

Friction torque and oil flow rate were measured simultaneously, with the displacement-measuring apparatus temporarily disconnected in order to eliminate the friction of the riders and the oil flow to them. The procedure of warming up and applying increments of load at constant speed was the same as in the displacement experiments. At each load, after the oil flow stabilized, the friction torquemeter was read, and the flow rate was determined by weighing the oil collected in periods of 1 to 2 minutes.

The following data were recorded for each load condition: Friction torque as indicated by the manometer, weight of oil flow from the test bearing, time of oil flow, capsule pressure, bearing temperature at critical locations, inlet oil pressure, speed, direction of rotation, inlet oil temperature, room temperature, and oil temperature after the heater. The same data were taken for the opposite direction of shaft rotation so that data could be averaged for the two rotations. As shown in table II, constant-speed runs at approximately 500, 1,200, and 5,000 rpm were conducted on the long journals 6A, 6B, and 6C. The maximum applied central load was 1,688 pounds with a maximum unit load on projected area of 594 pounds per square inch on shaft 6C. The maximum bearing temperature recorded was 181° F at 5,000 rpm.

RESULTS

The experimental data on eccentricity ratio, friction, and oil flow rate are shown in figures 1 to 4 in a form intended to be useful in the design of plain bearings with values of l/d as high as 2. The nondimensional coordinates shown are those determined from the analytical solution of reference 1. The coordinate point values shown were determined from the following expressions by using the known quantities from the experimental tests.

Load number:

$$\frac{1}{C_n} = \frac{p}{\mu N'}\left(\frac{c_d}{d}\right)^2\left(\frac{d}{l}\right)^2 \tag{3}$$

Eccentricity ratio:

$$\left.\begin{aligned} n = e/c_r &= \sqrt{(n_v)^2 + (n_h)^2} \\ n_v &= e_v/c_r \\ n_h &= e_h/c_r \end{aligned}\right\} \tag{4}$$

Bearing friction ratio:

$$\frac{F_b}{F_o} = \frac{F_b}{2\pi^2\mu N' l d(d/c_d)} \tag{5}$$

Couple friction ratio:

$$\left(\frac{\Delta F}{F_o}\right)\left(\frac{d}{l}\right)^2 = \left(\frac{F_j}{F_o} - \frac{F_b}{F_o}\right)\left(\frac{d}{l}\right)^2 \tag{6}$$

Oil flow factor:

$$q = \frac{Q}{\pi d l c_d (N'/2) n} \tag{7}$$

Inlet-oil-pressure number:

$$1/C_{p_o} = (1/C_n)(p_o/p) \tag{8}$$

Load Number

The experimental quantities in the load number (eq. (3)) are the load, viscosity, speed, diametral clearance, and bearing diameter and length. The unit load p on a projected area was determined from $p = P/ld$ and the total net load P applied by the piston was calculated from $P = 5.0(p_c - 12.5)$ where p_c is the capsule pressure acting on the piston area of 5.0 square inches. The tare weight of the bearing and attached apparatus is represented in these tests by a pressure of 12.5 pounds per square inch.

Viscosity values for the SAE 10 oil were taken from the curve of figure 9 and converted to reyns by dividing the centipoise values by 6.9×10^6. Oil film viscosity μ was determined from the temperature of thermocouple 4 located 1/16 inch from the bearing surface.

Diametral clearance at room temperature was determined from measurements of bearing and journal with electrolimit gages. For running conditions, clearance was determined by subtracting the change in clearance given in figure 10 from room-temperature clearance. The clearance in figure 10 represents the calculated clearance change caused by differential thermal expansion of bearing and journal as a function of the temperature gradient in the bearing housing. Thermocouples 4 and 9 were 1/16 inch and 2 inches, respectively, from the bearing surfaces, giving temperature differences $(t_4 - t_9)$ indicative of the gradient. The slope of the curve in figure 10 is approximately one-third of the slope of that used in reference 1. Additional study indicated that the earlier slope should be smaller. The differential expansion problem was reevaluated analytically by the method of Timoshenko (ref. 6).

Eccentricity Ratio

Calculations of experimental values of eccentricity ratio n in figure 1(a) were determined from the coordinate vertical and horizontal displacements of the shaft measured at the riders located beyond the ends of the bearing $1\frac{11}{16}$ inch from the center line of the bearing (cf. fig. 5). Eight observations of a coordinate displacement were averaged to determine the mean value at a given load. Readings of two dials, one at each end, as the loading was being increased and then decreased, gave four observations. Four more observations were available for the opposite direction of rotation.

In order to correct the values of the eccentricity ratio, the slight displacements at zero load and zero inlet oil pressure, at which it was assumed that the journal and bearing axes were coincident, were

averaged and subtracted from the averaged values of displacement under load. All displacements were halved because of the 2:1 multiplication of the measuring system.

Another correction was made to account for the effect of shaft deflection on displacement measurements. Calculations of shaft bending deflections were made assuming a uniformly distributed load over the length of the bearing and varying moments of inertia of the slightly stepped shaft. Deflection corrections were made on measured vertical displacements only. Because the journal within the bearing length is deflected to a fourth-degree parabola, the corrections were made to simulate the vertical displacement of an ideally straight journal located one-fifth of the height of the parabola below the apex. The vertical and horizontal components of eccentricity ratio n_v and n_h were calculated by dividing the corrected coordinate displacements by the radial clearance (eqs. (4)), and the eccentricity ratio n was calculated as the square root of the sum of the squares of the components.

The experimental data of eccentricity ratio shown in figure 1(b) for short bearings are from reference 1 and are shown for comparison with figure 1(a) for long bearings.

Bearing Friction Ratio

Experimental values of bearing friction ratio F_b/F_o in figure 2(a) were calculated from equation (5) in which the friction force F_b was determined from the mercury manometer readings of the torquemeter. Multiplication of the manometer values by the calibration factor F_c gave the friction torque. The average value of F_c was 0.475 pound-inch of torque per inch difference of mercury. Dividing the friction torque by the bearing radius gave the friction force F_b.

The experimental friction data for short bearings from reference 1 are shown in figure 2(b) for comparison with the long-bearing data in figure 2(a).

Couple Friction Ratio

The friction-ratio data shown in figure 2 represent measured values of friction acting on the bearing of the journal-bearing combination. As discussed in another section of this report, the friction ratio of the journal F_j/F_o may be obtained analytically by adding the couple friction ratio $\Delta F/F_o$ to the bearing friction ratio F_b/F_o. The couple friction ratio is of interest, since when multiplied by $(d/l)^2$ it is

a single-line function of the load number as shown in figure 3. The part of the friction on the rotating member which is due to the couple formed by the central load and the lateral displacement of the rotating member relative to the stationary member is represented nondimensionally by $\Delta F/F_o$.

The experimental data shown in figure 3 were reduced from data given by McKee and McKee (ref. 7) and Palsulich and Blair (ref. 8). Both investigators present friction data from tests in the four-bearing machine which measures journal friction. McKee and McKee present data in experimental curves of f against ZN/p with c_d/d and l/d ratios given, and Palsulich and Blair give tabular experimental data of $f(d/c_d)$ against $\mu N/p(d/c_d)^2$ with the l/d ratio given. These data are converted to F_j/F_o and l/C_n values by the following expressions:

$$f = f_j/P \tag{9}$$

$$F_o = 2\pi^2\mu N' ld(d/c_d) \text{ (Petroff friction)} \tag{10}$$

The McKee and McKee conversions are

$$\frac{l}{C_n} = \frac{6.9 \times 10^6 \times 60}{(ZN/p)(d/c_d)^2(l/d)^2} \tag{11}$$

$$\frac{F_j}{F_o} = \frac{fP}{2\pi^2\mu N' ld(d/c_d)}$$

$$= \frac{f(P/ld)}{2\pi^2\mu N'(d/c_d)}$$

$$= \frac{f}{2\pi^2}\left[\frac{p}{\mu N'}\left(\frac{c_d}{d}\right)\right]\frac{(c_d/d)(l/d)^2}{(c_d/d)(l/d)^2}$$

$$= \frac{f}{2\pi^2}\left(\frac{d}{c_d}\right)\left(\frac{l}{d}\right)^2\left(\frac{l}{C_n}\right) \tag{12}$$

The Palsulich and Blair conversions are

$$\frac{1}{C_n} = \frac{60}{\left[\frac{\mu N'}{p}\left(\frac{d}{c_d}\right)^2\right]\left(\frac{l}{d}\right)^2} \tag{13}$$

$$\frac{F_j}{F_o} = \frac{(fd/c_d)}{2\pi^2}\left(\frac{l}{d}\right)^2\left(\frac{1}{C_n}\right) \tag{14}$$

Values of $\Delta F/F_o(d/l)^2$ shown in figure 3 were determined from equation (6) using the experimental values of F_j/F_o and the analytical values of F_b/F_o from the analytical curve of figure 2.

Oil Flow Factor

The oil flow factor q in figure 4(a) was calculated from equation (7) as in reference 1. The oil flow rate Q in cubic inches per second was converted from the measured flow in pounds per minute using the specific gravity of the oil at bearing temperature. Because displacement measurements were not simultaneous with measurements of oil flow, values of eccentricity ratio n in equation (7) were taken from the experimental data of figure 1(a) for corresponding test conditions. The inlet-oil-pressure number $1/C_{p_o}$, against which q is plotted in figure 4, was determined from the load number and the ratio of inlet oil pressure p_o to unit bearing pressure p as in equation (8).

Experimental oil flow factors for the short bearings of reference 1 are shown in figure 4(b) for comparison with the long-bearing data in figure 4(a).

Experimental data from McKee (ref. 9) for a bearing with a single oil hole are also shown in figures 4(a) and 4(b) and compare well with the experimental data of this investigation. Additional McKee data from reference 9 enable a curve to be drawn for a bearing having an axial oil groove which is somewhat shorter than the length of the bearing.

ANALYSIS AND DISCUSSION

The dependence of eccentricity ratio, friction, and oil flow on the load number $1/C_n$ is shown in figures 1 to 4. The $(l/d)^2$ term

in the load number serves to reduce experimental data for various values of l/d to nearly a single curve. A single exception is the curve for eccentricity ratio in figure 1(a) in which the experimental data cluster near a single line only if the $(l/d)^2$ term in the load number is taken as unity for the long bearings for which l/d is greater than 1. For the bearing friction ratio in figure 2, the couple friction ratio in figure 3, and the oil flow factor in figure 4, the $(l/d)^2$ term appears to be basically applicable for bearings with values of l/d from 1/4 to 2.

Figures 1 to 4 are intended to serve as design charts for bearings having load numbers up to 100 covered by the experimental data from these tests. As shown in figure 1(a), eccentricity ratios averaging $n = 0.93$ were attained experimentally at load numbers of approximately 90. Above this, the value of eccentricity ratio apparently becomes asymptotic to $n = 1.00$ as the load number becomes infinite.

Eccentricity Ratio

Two sets of experimental data on eccentricity ratio appear in figure 1(a) and are shown separately in figures 1(b) and 1(c). Those in figure 1(b) are for the long bearings of $l/d = 3/4$ to 2 from the experiments using shafts 6A to 6E. In figure 1(c) are data from reference 1 for short bearings of $l/d = 1/4$ to 1. It may be seen that the device of assuming values of l/d of unity for the long bearings makes the long- and short-bearing eccentricity data nearly coincident. The unit bearing pressure on projected area p appears in the load number, rather than the total load, and the above device can be interpreted to mean that the allowable unit bearing load is practically independent of l/d for values of l/d above 1 but that for values of l/d less than 1 the allowable unit bearing load falls as the square of l/d.

The experimental data of figures 1(b) and 1(c) are also shown in figures 11(a) and 11(b) using the capacity number C_n as the abscissa rather than its reciprocal, the load number $1/C_n$. In figure 11, the useful load region is compressed in the range of abscissas from 0 to 0.1, whereas in figures 1(b) and 1(c), which use the load number $1/C_n$, this region extends from 10 to infinity in proportion to the unit load. The load-number method of plotting avoids devoting 90 percent of the graph to the light-load region below a load number of 10.

The experimental values of eccentricity ratio are materially larger than those indicated by the analytical curve of the short-bearing approximation. Some of the difference between the curves may possibly be due to the sensitivity of the experimental data to small errors in determination of either the cold clearance or the clearance at running temperature.

Usual measurements of the bearing clearance tend to give readings at the top of the waviness of the surfaces, rather than the effective diameter. An analytical correction for the change of clearance at running temperature was used in calculating the experimental data and should be included in making use of the curves. An appreciation of the magnitude of the change in eccentricity corresponding to a difference in n value of 0.90 to 0.95 is given by considering that this represents a change in displacement of about 0.000050 inch in these tests.

Perhaps the most important factor related to the difference between the analytical curve given by the short-bearing approximation and the experimental data is the omission in the analytical solution of the effect of the circumferential pressure differential on the leakage in the circumferential direction of the oil film. The analytical solution includes the side leakage and the circumferential flow due to rotation, but the omission of part of the circumferential leakage mentioned would theoretically cause the experimental value of n to be above the analytical curve by a small unknown amount. It is also possible that the difference between the analytical and experimental curves is related to the use of a temperature near the bearing surface to obtain viscosity, rather than the temperature of the oil film. A constant viscosity was also used, rather than one changing from point to point with the oil film temperature and pressure.

All of these factors are representative of methods that would commonly be used in predicting bearing performance from the curves. The experimental curve is thus representative of the effect to be expected when these methods are used.

Considering these factors, a single experimental line is shown in figure 1(a) which is the average of all of the data in both curves 1(b) and 1(c). While figures 1(b) and 1(c) differ slightly in the light-load region, the single experimental line of figure 1(a) is considered to be a practical interpretation of the data. For practical use and to be on the conservative side, it is recommended that the experimental curve in figure 1(a) be used, rather than the analytical curve.

In figure 1(a) the experimental values are about 15 percent greater than the analytical ones for load numbers between 10 and 100. For load numbers above about 60 it is an advantage to have an approximation that becomes asymptotic to a value of n of 1 in the same way that the analytical curve does. For values of the load number greater than 100 the experimental value evidently lies between the analytical value larger than 0.93 as it becomes asymptotic and 1. This effect can be obtained by adding $0.5(1 - n)$ to the analytical value of n.

Blending of $(l/d)^2$ transition.- The device of considering the $(l/d)^2$ term in the load number as having a value of 1 for values of l/d

greater than 1 can be expressed mathematically by considering the l/d term to have an unknown exponent of x. The value of the exponent x changes from 2 for values of l/d less than 1 to zero for l/d greater than 1. The transition of the exponent from a value of 2 to zero can then be considered to occur in a smooth manner, and the shape of the transition curve and the range of l/d in which the transition occurs remain to be determined experimentally.

The difference between a smooth blending of the change in the exponent x and an abrupt change is minimized by the fact that the transition occurs in the neighborhood of a value of l/d of 1, where the value of $(l/d)^x$ is 1 regardless of the value of x. The abrupt change may be sufficiently accurate for practical purposes, as indicated by the following arbitrary example. Assume that the value of x should be 2 at $l/d = 1$ and then decreases linearly to zero at $l/d = 1.2$ where $(1.2)^0 = 1$. The maximum change occurs at a value of l/d of about 1.1 where $(l/d)^x = (1.1)^1$, with the effect decreasing in either direction from 1.1. Thus the maximum effect of this method of blending is a change in load number of about 10 percent at midrange, if the range in which the transition occurs is 0.2 points of l/d.

Analytical curves.- Analytically, information on eccentricity ratio against load number for short bearings is available from the solutions by the short-bearing approximation (ref. 1) and by the method of Cameron and Wood (ref. 2). These are shown as the upper group of curves in figures 12 and 13. The curve from the short-bearing approximation is a single curve theoretically applicable to short bearings. The Cameron and Wood exact solution of Reynolds' equation gives points indicating separate curves for $l/d = 1/4$, $1/2$, and 1. A comparison of these upper curves with the experimental curve which is repeated in figure 13 shows that the plotting of the data as a function of the load number using the $(l/d)^2$ term for $l/d < 1$ is justifiable. The use of the load number in this manner permits direct comparison of analytical and experimental data for all values of l/d on one curve. The locations of the Cameron and Wood points are also found to be in relatively close agreement with the experimental curve and substantiate the use of the curve in figure 1(a) for practical purposes when using the load number as a parameter.

In figures 12 and 13, the lower group are analytical curves for infinite values of l/d from two solutions by Sommerfeld (ref. 3) and one from Cameron and Wood (ref. 2). These curves for infinite values of l/d of necessity refer to the abscissa scale labeled $1/S$ since no finite values of l/d are available. It can also be said that the curves are plotted in accordance with the device that infinitely long bearings are considered to be of $l/d = 1$, such that the Sommerfeld number applies rather than the capacity number. It is interesting that the infinite-bearing curves agree with the short-bearing curves at the

high load numbers although they are greatly divergent at low load numbers. It is perhaps for this reason that use of the Sommerfeld solution for bearings with $l/d = 1$ has been successful. However, for bearings shorter than $l/d = 1$, use of the Sommerfeld solution would be less conservative as l/d decreases from 1.

The differences in the three curves shown for infinite values of l/d are a result of different assumptions as to the circumferential extent of pressurized oil film. The Sommerfeld solution based on a 2π or 360° extent of the film assumes that negative pressures contribute to the load capacity of a bearing. In the Cameron and Wood solution, the film extent is somewhat greater than 180°, depending upon assumptions regarding boundary conditions of the circumferential pressure gradient. The third curve shown is based on Sommerfeld's pressure-distribution function for an infinite bearing, but the integrations to determine load capacity as a function of n are based on a pressurized film of π or 180° extent, thus eliminating the effect of negative pressures. Equations (15) and (16) below show the difference in the analytical functions of the Sommerfeld type on the basis of extent of the oil film. For the 2π film

$$S = \frac{\mu N'}{p}\left(\frac{d}{c_d}\right)^2 = \frac{\left(2 + n^2\right)\left(1 - n^2\right)^{1/2}}{12\pi^2 n} \tag{15}$$

For the π film

$$S = \frac{\mu N'}{p}\left(\frac{d}{c_d}\right)^2 = \frac{\left(2 + n^2\right)\left(1 - n^2\right)}{6\pi n\left[\pi^2\left(1 - n^2\right) + 4n^2\right]^{1/2}} \tag{16}$$

The integrations for the determination of equation (16) are shown in the appendix.

Comparing the lower group of curves in figure 13 which refer to bearings of infinite values of l/d with experimental data of l/d of 2 or less seems to indicate that the assumption of l/d of infinity gives too low a value of eccentricity ratio at light loads. The assumption of infinite values of l/d eliminates the effect of end leakage on the pressure distribution in the oil film. The spread of the data in figure 1(b) for bearings of l/d of 1.5 and 2 is closer to the upper group of curves at light loads than to the curves for infinite values of l/d.

Bearing Friction

Curves of bearing friction ratio F_b/F_o for long bearings and short bearings are shown, respectively, in figures 2(a) and 2(b). Both curves show the experimental data plotted as a function of the load number $1/C_n$ in which the $(l/d)^2$ term is included. It may be seen that the short- and long-bearing experimental data, when compared with the analytical curve, are nearly coincident without distinguishing between short or long bearings in the load number as is done in the curves of eccentricity ratio. The curve obtained by means of the device of using $1/S$ for the long bearings in which l/d is taken as unity is shown in figure 14(a) for the same experimental data of figure 2(a). It may be seen that the same data are in better agreement with the short-bearing analytical curve in figure 2(a) than in figure 14(a). It is interesting, however, that the experimental data for long bearings in figure 14(a) are in fairly reasonable agreement with the analytical curves for infinite values of l/d by Cameron and Wood (ref. 2) and by the Sommerfeld solution for 180° film extent of this report.

Analytical curves for bearing friction ratio from the solutions of Cameron and Wood (ref. 2) and the short-bearing approximation (ref. 1) agree well when plotted against load number $1/C_n$ for short bearings. These are shown in figure 14(b) for $l/d = 1/4$, $1/2$, and 1. Originally, the Cameron and Wood curves for friction were plotted on coordinates of $f(r/c_r)$ against the Sommerfeld number. A replotting of their curves of bearing friction as in figure 14(b) shows the influence of $(l/d)^2$ in drawing the curves for $l/d = 1/4$, $1/2$, and 1 together.

Journal Friction

The Cameron and Wood curves of journal friction ratio F_j/F_o against load number in figure 15(a) show a greater divergence with l/d than the bearing friction curves in figure 14(b). They also show that the difference between journal friction and bearing friction may be great for high load numbers and large values of l/d. The same curves plotted on coordinates of $f(r/c_r)$ against S also show a difference between journal and bearing friction, but this difference is difficult to distinguish since the high load values plot near the origin. By plotting friction ratio against load number, the difference between journal and bearing friction is shown more clearly.

Analytically, the short-bearing approximation does not indicate a difference between journal and bearing friction because of the assumption that the circumferential velocity profile in the oil film is linear. In this respect, the agreement of the Cameron and Wood and short-bearing curves for bearing friction is of considerable interest. From equilibrium

conditions, the bearing friction torque is theoretically less than the journal friction torque by the couple $Pe \sin \phi$. Curves for journal friction can be determined from relationships of the short-bearing approximation by adding this couple to the friction torque of the bearing. The curves of journal friction in figure 15(a), labeled short-bearing approximation, are based on this addition in accordance with the following analysis.

The difference between journal and bearing friction torque $\Delta F(d/2)$ is equal to the couple of the load P and the lateral displacement of the journal $e_h = e \sin \phi$:

$$\Delta F \frac{d}{2} = Pe \sin \phi \tag{17}$$

In terms of friction ratio:

$$\frac{\Delta F}{F_o} = \frac{Pe \sin \phi}{F_o}\left(\frac{2}{d}\right) \tag{18}$$

Substitution of $P = \mu N'(d/c_d)^2(l/d)^2(1/C_n)ld$, $e = n(c_d/2)$, and the Petroff friction $F_o = 2\pi^2 \mu N' l d(d/c_d)$ gives

$$\frac{\Delta F}{F_o} = \frac{n \sin \phi}{2\pi^2} \frac{(l/d)^2}{C_n} \tag{19}$$

$$\frac{\Delta F}{F_o}\left(\frac{d}{l}\right)^2 = \frac{n \sin \phi}{2\pi^2} \frac{1}{C_n} \tag{20}$$

Since $\sin \phi$ and the load number $1/C_n$ are functions of n as given in reference 1, the curve of $(\Delta F/F_o)(d/l)^2$ against load number from equation (20) is a single line as shown in figure 3.

The ratio $\Delta F/F_o$ is the couple friction ratio which is added to the bearing friction ratio to obtain the journal friction ratio

$$\frac{F_j}{F_o} = \frac{F_b}{F_o} + \frac{\Delta F}{F_o} \tag{21}$$

As shown in figure 15(a), the plot of journal friction ratio against load number gives a family of curves which are in close agreement with the curves from the Cameron and Wood solution.

Experimental data on journal friction.- Since experimental data of journal friction are not available from this investigation, data from McKee and McKee (ref. 7) and Palsulich and Blair (ref. 8) are shown in figures 15(b) to 15(f) for comparison with the analytical curves from equations (19) and (21). Data from these investigators were obtained from the four-bearing machine which measures the friction torque of the journal.

McKee and McKee present data for a $1\frac{1}{4}$-inch-diameter bearing with a range of clearance ratios from 0.0005 to 0.0040 for $l/d = 1/4$, $1/2$, $3/4$, 1, and 2.8. Comparatively light loads were used, but high load numbers of the order of 500 were obtained at low rotative speeds. These data are shown in reference 7 as experimental curves, rather than points, plotted on coordinates of f (friction coefficient = F/P) against ZN/p. Since the l/d and c_d/d information are given with the curves, conversion of the data to F_j/F_o and $1/C_n$ coordinates is possible as shown in figures 15(b) to 15(e).

Figures 15(b) and 15(c) compare the McKee and McKee data with equation (21) for the short bearings of $l/d = 1/4$ and $1/2$ and figures 15(d) and 15(e) compare them for $l/d = 1$ and 2.8. These curves show that agreement of the analytical and experimental curves is better for $l/d = 1/2$, 1, and 2.8 than for the very short bearing of $l/d = 1/4$ where the loads were very small. Since one set of data for $l/d = 1$ is given in tabular form in reference 7, it is possible to show point data in figures 15(d) and 15(e) for the friction rise beyond the hook point in the region of boundary lubrication. The sequence of data points around the hook is shown by the ZN/p curve inset in figure 15(d). The points above the hook rapidly leave the scale of the F_j/F_o curve. The hook point is indicated on the F_j/F_o curve by an increase of slope of the line which tends to rise almost vertically to points off the vertical scale. The more rounded the hook on the ZN/p curve, the more gradual the change of slope in the F_j/F_o curve.

High load numbers are shown in the experimental curves of figures 15(b) and 15(c) for $l/d = 1/4$ and $1/2$ because of the influence of the $(l/d)^2$ term in the load number, and the maximum load numbers for $l/d = 1$ and 2.8 are much smaller.

Palsulich and Blair present experimental data from a four-bearing machine similar in principle to the McKee and McKee machine but modified to operate at higher loads and greater speeds. Data are presented for

a bearing approximately 2 inches in diameter and $1\frac{1}{4}$ inches long with a diametral clearance of 0.004 inch. Speeds as high as 5,000 rpm and unit loads to 4,000 pounds per square inch were used. The experimental data are presented in reference 8 using coordinates of $f(r/c)$ and S, where c is the radial bearing clearance. These may be converted to F_j/F_o and l/C_n values as shown in figure 15(f). An exact value of l/d is not given, but an inspection of the tabular data indicates that the bearing was $2\frac{1}{16}$ by $1\frac{1}{4}$ inches with $l/d = 0.607$. Figure 15(f) shows the comparison of experimental data with equation (21). Load numbers in excess of 1,000 were obtained as shown. The experimental data agree well with the analytical curve below a load number of 100 but are between the analytical curves of $l/d = 0.607$ and 1 at the high load numbers. In reference 8, the plot of the friction data on $f(r/c)$ and S coordinates did not exhibit a hook point even at the very high load numbers.

An important feature of the analytical curves in figure 15(f) is that on the coordinates shown they indicate journal friction to be several hundred percent of the bearing friction at high load numbers and high values of l/d.

Both the McKee and McKee and Palsulich-Blair data were used to determine the couple friction ratio $\Delta F/F_o$ for plotting $\Delta F/F_o(d/l)^2$ as in figure 3. Experimental data of couple friction ratio were determined by subtracting the short-bearing analytical value of bearing friction ratio from the experimental journal friction ratio. As shown in figure 3, most of the experimental data are above the analytical curve. The McKee and McKee curves which did not continue beyond the hook are in relatively good agreement with the analytical line, except for the data at $l/d = 1/4$, which are off the scale. The method of plotting the difference of journal and bearing friction as in figure 3 magnifies the differences shown in figures 15(b) to 15(e) and is worthy of wider acceptance as a tool to magnify the spread of friction data at high loads which are hidden near the origin of the ZN/p curves.

Analytical curves: infinite values of l/d.- Analytical curves of bearing and journal friction for bearings of infinite length are shown in figure 16 on coordinates of friction ratio and $1/S$. The three sets of curves shown are derived from the analytical solutions of Cameron and Wood (ref. 2) and Sommerfeld. Two sets of the analytical curves are based on the Sommerfeld pressure-distribution function, one set as given by Sommerfeld (ref. 3) for a 2π or 360° pressurized film and one set for a π or 180° pressurized film as determined in the analysis of the appendix. In all three solutions, the friction force F is determined from integrations of film shearing stresses over 360°. However, the effect of film pressure on the shearing stresses depends upon the angular extent of the pressurized film. As shown in

the appendix, the friction-ratio curves for the Sommerfeld π case may be determined from the sum of two integrations, one from the Sommerfeld shearing stress function for the pressurized film of π extent, and one from the short-bearing approximation function for the nonpressurized film of π extent where a linear circumferential velocity profile is assumed. Equations (22) and (23) below show the difference in form of the friction-ratio functions of the 2π and π cases of the Sommerfeld solution. For the 2π film

$$\left.\begin{aligned} \frac{F_b}{F_o} &= \frac{2\left(1 - n^2\right)}{\left(2 + n^2\right)\left(1 - n^2\right)^{1/2}} \\ \frac{F_j}{F_o} &= \frac{2\left(1 + 2n^2\right)}{\left(2 + n^2\right)\left(1 - n^2\right)^{1/2}} \end{aligned}\right\} \tag{22}$$

For the π film

$$\left.\begin{aligned} \frac{F_b}{F_o} &= \frac{1}{2}\,\frac{\left(4 - n^2\right)}{\left(2 + n^2\right)\left(1 - n^2\right)^{1/2}} \\ \frac{F_j}{F_o} &= \frac{1}{2}\,\frac{\left(4 + 5n^2\right)}{\left(2 + n^2\right)\left(1 - n^2\right)^{1/2}} \end{aligned}\right\} \tag{23}$$

As shown in figure 16, the Sommerfeld π curve and the Cameron and Wood curve for bearing friction are almost identical in the load-number range shown and are in fair agreement with the experimental data for long bearings in figure 14(a). The analytical curves for journal friction are somewhat divergent, the Sommerfeld 2π curve giving the largest friction values.

The Sommerfeld 2π solution shows the greatest difference between bearing and journal friction as shown in figure 16. This is a direct result of the assumption in the 2π solution that negative pressures contribute to the load-carrying capacity of a bearing and cause displacements always normal to the load line as shown in the clearance circle diagram of figure 17. The moment arm of the friction couple is always greater therefore in the 2π solution than the moment arms of the π solution or the Cameron and Wood solution for the same value of n.

If infinite l/d analytical solutions are to be used in long-finite-bearing applications, it would seem that the Cameron and Wood and Sommerfeld π solutions are the most realistic since most experimenters have reported displacement curves of the semicircular form shown in figure 17.

The displacement curve for the Sommerfeld π case shown in figure 17 is based on equation (24) determined from the analysis in the appendix:

$$\tan \phi = \frac{\pi\left(1 - n^2\right)^{1/2}}{2n} \tag{24}$$

Oil Flow

The experimental data for oil flow factor q shown in figure 4(b) are from reference 1 but are replotted in order to show oil flow rate as a reciprocal function. The inlet-oil-pressure number $1/C_{p_o}$ contains the load number $1/C_n$ and the ratio of oil supply pressure p_o to the unit bearing pressure. The curve presented in reference 1 is shown for comparison in figure 18. Both curves show the experimental data for short bearings having a single oil feed hole located opposite the load. Also shown are data from tests by McKee (ref. 9) for bearings with a single oil hole and for bearings with an axial oil groove. The curves of figure 4(b) apply to bearings of l/d up to 2, although only the short-bearing data are shown because the long-bearing data plot so near the origin. An enlarged plot with scales five times size is shown separately in figure 4(a) with data for $\frac{l}{d} = 1$, $1\frac{1}{2}$, and 2. The solid line drawn through the experimental data for long bearings with a single oil hole in figure 4(a) is the same line shown in figure 4(b).

As indicated in reference 1, the oil flow factor q (eq. (7)) is the ratio of total oil flow rate Q issuing from the ends of the bearing to the analytically determined flow rate $\pi dlc_d(N'/2)n$ discharging from the pressurized 180° of the bearing. The analytical flow rate, based on the short-bearing approximation, may be viewed as a volumetric displacement rate in cubic inches per second. It is equal to the difference between the flow rate entering at the point of maximum film thickness and that leaving the bearing at the point of minimum film thickness, under the effects of rotation and viscosity, at zero circumferential pressure gradient. The total flow rate Q was determined by experimental measurement. By empirical methods of plotting the experimental data, it was found that the oil flow factor q appears to be a function of the inlet-pressure capacity number C_{p_o}:

$$C_{p_o} = \left(\frac{\mu N'}{p_o}\right)\left(\frac{d}{c_d}\right)^2\left(\frac{l}{d}\right)^2 \qquad (25)$$

However, the reciprocal form of the curves of figures 4(a) and 4(b) seems to give even better correlation as a function of the inlet-oil-pressure number $1/C_{p_o} = \left(1/C_n\right)\left(p_o/p\right)$ as given in equation (8).

Figures 4(a) and 4(b) are intended to serve as a means for the determination of oil flow rate Q from known conditions involving the variables in the load number and the known oil feed pressure p_o. It should be noticed that the device of taking l/d as 1 for values of l/d greater than 1 is not used for the oil flow curves, except indirectly when the value of n so obtained enters into the calculation of the analytical part of the oil flow rate.

Figure 4 is not intended to be used as a device to predict the oil supply pressure p_o. No criterion, other than operating temperature, is available which specifies the minimum value of oil flow factor q or oil flow rate Q. Cases of bearings performing successfully on thick films under starved conditions of oil flow are known, but the degree to which starvation can be tolerated is not known. Figure 4(a) indicates that bearings having l/d greater than 1 are apt to have an oil flow factor q less than 1, which may be an indication that oil grooves are desirable for long bearings to increase oil flow and lower operating temperature as indicated by figure 37 in reference 1.

USE OF CURVES

Figures 1 to 4 may be used to predict eccentricity, minimum film thickness, bearing and journal friction, journal power loss, and oil flow rate for bearings to $l/d = 2$. However, the variables contained in the load number and inlet-oil-pressure number must be known, including the running temperature of the bearing which determines film viscosity. Inlet oil pressure must also be known. For bearings of l/d of 1 or less, the load number may be calculated including the $(l/d)^2$ term to determine the above-named performance characteristics. However, for bearings of l/d greater than 1, two load numbers are required. The load number $1/S$ without the $(l/d)^2$ term is used to determine the eccentricity ratio n from figure 1(a) which is used in the calculation of oil flow rate Q from figure 4. Load number $1/C_n$ including $(l/d)^2$

is required in the determination of bearing and journal friction, couple friction ratio, and inlet-oil-pressure number.

A method of approximating maximum bearing temperature by the use of a heat balance diagram is described in reference 1. Figures 2 and 3 can be used to estimate bearing friction and the increment of couple friction to obtain the friction of the rotating element which gives the power loss and heat generated. Figure 4 gives oil flow data for use in estimating the heat carried away by the oil flow.

CONCLUSIONS

The following conclusions may be drawn from the results of the experimental investigation of eccentricity ratio, friction, and oil flow of long and short journal bearings with load number charts:

1. The performance of plain bearings under steady load is reduced to single-line charts covering the usual range of length-to-diameter ratios l/d from 1/4 to 2 by the use of the load number in the manner described.

2. Inclusion of the $(l/d)^2$ term in the load number collects the experimental data in a single line in all cases except one of eccentricity ratio where l/d values greater than 1 are taken as unity in computing the load number.

3. The $(l/d)^2$ term is included in the load number to determine the friction-ratio and the oil flow factor from the figures.

4. The addition of the increment of friction torque formed by the sideward displacement of the load to the friction torque on the stationary element to predict the friction torque of the rotating element, heat generated, and power loss is supported by analytical curves and experimental data of other investigators who have measured journal friction.

5. The method of plotting friction in two parts, the bearing friction ratio F_b/F_o and the increment of the load couple $\Delta F/F_o$, permits hydrodynamic friction to be determined from single-line curves which have been shown to apply to the usual ranges of clearance and length-to-diameter ratio. The prediction of friction from ratios related to the Petroff friction at no load is more rational than the use of a friction coefficient based on load.

6. The reciprocal form of the load number $1/C_n$ is preferable to C_n as a parameter. The load number increases in direct proportion to

unit load and is properly weighted to have meaning as a quantitative measure of relative loading. The area on the graph devoted to the light-load region is minimized, and the effect of high load numbers is shown more clearly.

Cornell University,
Ithaca, N. Y., August 20, 1954.

APPENDIX

INTEGRATIONS FOR SOMMERFELD π CASE

The following integrations giving eccentricity ratio, attitude angle, and friction ratio are based on the Sommerfeld pressure-distribution function (ref. 3) for a bearing without end leakage. However, a basic change in assumptions is made concerning the circumferential extent of the pressurized film. Sommerfeld's integration to determine the resultant force or load P includes the negative pressure region of the diverging wedge of the oil film as well as the positive pressure region of the converging wedge. In effect, a working film of 2π or 360° is assumed such that the negative pressure region contributes to the support of the load. The following analysis is based on the assumption that support of the load by negative pressures is negligible and that the working film is in the converging wedge and is of π or 180° in circumferential extent. The same assumption is made in the short-bearing approximation (ref. 1).

Eccentricity-Ratio Function

The following equation is the pressure-distribution function given by Sommerfeld in which p_s represents the datum film pressure at the leading and trailing ends of the converging wedge of the oil film:

$$p_{film} = \frac{6\mu Ur}{c_r^2}\left[\frac{n \sin\theta(2 + n\cos\theta)}{(2 + n^2)(1 + n\cos\theta)^2}\right] + p_s \qquad (27)$$

In the following steps p_s is assumed to be zero gage pressure such that equation (27) gives film gage pressures. The angular variable θ is measured from the location of maximum film thickness.

The X and Y coordinates are chosen parallel and perpendicular, respectively, to the line joining the journal and bearing centers which are at an eccentricity e. The orthogonal components of the resultant P are P_X and P_Y. The following integrations over π radians determine the relationship of the load P as a function of eccentricity ratio n:

$$P_X = l \int_{\theta=0}^{\theta=\pi} p_{film} r \cos\theta \, d\theta$$

$$= 6\mu U l \left(\frac{r}{c_r}\right)^2 \int_0^{\pi} \frac{n \sin\theta \cos\theta (2 + n\cos\theta)}{(2 + n^2)(1 + n\cos\theta)^2} \, d\theta$$

$$= \mu U l \left(\frac{d}{c_d}\right)^2 \frac{12n^2}{(2 + n^2)(1 - n^2)} \tag{28}$$

$$P_Y = l \int_0^{\pi} p_{film} r \sin\theta \, d\theta$$

$$= 6\mu U l \left(\frac{r}{c_r}\right)^2 \int_0^{\pi} \frac{n \sin^2\theta (2 + n\cos\theta)}{(2 + n^2)(1 + n\cos\theta)^2} \, d\theta$$

$$= \mu U l \left(\frac{d}{c_d}\right)^2 \frac{6\pi n}{(2 + n^2)(1 - n^2)^{1/2}} \tag{29}$$

$$P = \sqrt{P_X^2 + P_Y^2}$$

$$= 6\mu U l \left(\frac{d}{c_d}\right)^2 \frac{n}{(2 + n^2)(1 - n^2)} \left[n^2(4 - \pi^2) + \pi^2\right]^{1/2} \tag{30}$$

Substituting $P = pld$ and $U = \pi dN'$

$$S = \frac{\mu N'}{p}\left(\frac{d}{c_d}\right)^2 = \frac{(2 + n^2)(1 - n^2)}{6\pi n\left[\pi^2(1 - n^2) + 4n^2\right]^{1/2}} \tag{31}$$

Equation (31) is the same as equation (16) in the body of this report. The analytical curves of eccentricity ratio against Sommerfeld number representing equation (31) are shown in figures 12 and 13.

Attitude Angle

The angular location of the resultant P with respect to the X-axis, or attitude angle ϕ, is determined from the following expression:

$$\tan \phi = \frac{P_Y}{P_X}$$

$$= \frac{\pi\left(1 - n^2\right)^{1/2}}{2n} \tag{32}$$

The attitude angle also gives the angular position of the minimum film thickness relative to the load line as shown in figure 17. Equation (32), which is the same as equation (24), shows the displacement path in figure 17 to be nearly semicircular rather than straight as in the Sommerfeld 2π solution.

Friction Ratio

Equations for friction forces on the bearing and journal are given by Sommerfeld (ref. 3) for the 2π radians or 360° extent of the pressurized film. To determine the friction forces F_b' and F_j' on bearing and journal, respectively, for the Sommerfeld π case, with a pressurized film extending 180° or 1/2 of the arc, half of the values given by Sommerfeld may be used to represent the effect of the pressurized half of the oil film on friction:

$$F_b' = \mu U l \left(\frac{d}{c_d}\right) \frac{2\pi\left(1 - n^2\right)}{\left(2 + n^2\right)\left(1 - n^2\right)^{1/2}} \tag{33}$$

$$F_j' = \mu U l \left(\frac{d}{c_d}\right) \frac{2\pi\left(1 + 2n^2\right)}{\left(2 + n^2\right)\left(1 - n^2\right)^{1/2}} \tag{34}$$

To equations (33) and (34) must be added the friction of the non-pressurized film in which the velocity profile is linear. Half of the values given by the equations of the short-bearing approximation may be used to represent this friction F':

$$F' = \mu U l \left(\frac{d}{c_d}\right) \frac{\pi}{\left(1 - n^2\right)^{1/2}} \tag{35}$$

The total friction forces F_b and F_j are the sums of equations (33) and (35) and equations (34) and (35):

$$\begin{aligned} F_b &= F_b' + F' \\ &= \mu U l \left(\frac{d}{c_d}\right) \left[\frac{2\pi\left(1 - n^2\right)}{\left(2 + n^2\right)\left(1 - n^2\right)^{1/2}} + \frac{\pi}{\left(1 - n^2\right)^{1/2}} \right] \\ &= \mu U l \left(\frac{d}{c_d}\right) \frac{\pi\left(4 - n^2\right)}{\left(2 + n^2\right)\left(1 - n^2\right)^{1/2}} \end{aligned} \tag{36}$$

$$\begin{aligned} F_j &= F_j' + F' \\ &= \mu U l \left(\frac{d}{c_d}\right) \left[\frac{2\pi\left(1 + 2n^2\right)}{\left(2 + n^2\right)\left(1 - n^2\right)^{1/2}} + \frac{\pi}{\left(1 - n^2\right)^{1/2}} \right] \\ &= \mu U l \left(\frac{d}{c_d}\right) \frac{\pi\left(4 + 5n^2\right)}{\left(2 + n^2\right)\left(1 - n^2\right)^{1/2}} \end{aligned} \tag{37}$$

Dividing F_b and F_j by the load P in equations (36) and (37) results in equations in terms of coefficient of friction f_b and f_j. Substituting $U = \pi d N'$, $P = p l d$, and $S = (\mu N'/p)(d/c_d)^2$,

$$f_b(d/c_d) = S \frac{\pi^2\left(4 - n^2\right)}{\left(2 + n^2\right)\left(1 - n^2\right)^{1/2}} \tag{38}$$

$$f_j(d/c_d) = S \frac{\pi^2\left(4 + 5n^2\right)}{\left(2 + n^2\right)\left(1 - n^2\right)^{1/2}} \tag{39}$$

To obtain friction in terms of friction ratio, equations (36) and (37) are divided by the Petroff value of friction F_o:

$$\frac{F_b}{F_o} = \frac{\mu U l (d/c_d)}{2\pi^2 \mu N' l d (d/c_d)} \frac{\pi(4 - n^2)}{(2 + n^2)(1 - n^2)^{1/2}}$$

$$= \frac{1}{2} \frac{(4 - n^2)}{(2 + n^2)(1 - n^2)^{1/2}} \tag{40}$$

$$\frac{F_j}{F_o} = \frac{1}{2} \frac{(4 + 5n^2)}{(2 + n^2)(1 - n^2)^{1/2}} \tag{41}$$

Equations (40) and (41) are the same as equations (23) and are shown plotted in figure 16 for comparison with the Sommerfeld 2π solution.

REFERENCES

1. DuBois, George B., and Ocvirk, Fred W.: Analytical Derivation and Experimental Evaluation of Short-Bearing Approximation for Full Journal Bearings. NACA Rep. 1157, 1953. (Supersedes NACA TN's 2808 and 2809.)

2. Cameron, A., and Wood, W. L.: The Full Journal Bearing. Proc. Institution Mech. Eng. (London), vol. 161, W.E.P. Nos. 47-54, 1949, pp. 59-72.

3. Sommerfeld, A.: The Hydrodynamic Theory of Lubrication Friction. Zs. Math. und Phys., vol. 50, nos. 1 and 2, 1904, pp. 97-155.

4. DuBois, G. B., Ocvirk, F. W., and Wehe, R. L.: Experimental Investigation of Misalining Couples and Eccentricity at the Ends of Misalined Plain Bearings. NACA TN 3352, 1954.

5. Wilcock, D. F., and Rosenblatt, Murray: Oil Flow, Key Factor in Sleeve-Bearing Performance. Trans. A.S.M.E., vol. 74, no. 5, July 1952, pp. 849-866.

6. Timoshenko, S.: Strength of Materials. Part II - Advanced Theory and Problems. Second ed., D. Van Nostrand Co., Inc., 1941, pp. 258-264.

7. McKee, S. A., and McKee, T. R.: Friction of Journal Bearings as Influenced by Clearance and Length. Trans. A.S.M.E., APM-51-15-161, vol. 51, Aug. 1929, pp. 593-595.

8. Palsulich, J., and Blair, R. W.: Testing of Highly Loaded Sleeve Bearings. SAE Jour., vol. 54, no. 9, Sept. 1946, pp. 481-490.

9. McKee, S. A.: Oil Flow in Plain Journal Bearings. Trans. A.S.M.E., vol. 74, no. 5, July 1952, pp. 841-848.

TABLE I.- EXPERIMENTAL CONDITIONS IN DISPLACEMENT EXPERIMENTS

[$1\frac{3}{8}$-in.-diam. steel journal and bronze bearing; SAE 10 oil supplied through a 1/8-in.-diam. oil hole opposite central load]

Shaft	l/d	c_d, in.	$\frac{c_d}{d}$	Speed, N, rpm	Maximum load, P, lb	Maximum unit load, p, lb/sq in.	Maximum bearing temp., T_4, °F	Oil inlet pressure, p_o, lb/sq in.
6A	2	0.00252	0.00183	500	1,007	266	125	80
				1,000	1,293	342	129	80
				2,500	1,438	380	149	140
				5,000	1,538	406	175	140
				5,000	1,663	438	170	120
6B	2	0.00376	0.00273	500	843	223	129	80
				1,000	1,007	266	132	80
				5,000	1,438	380	156	140
				5,000	1,438	380	169	140
6C	$1\frac{1}{2}$	0.00196	0.00142	1,200	938	329	134	80
				1,200	388	137	128	80
				1,200	938	329	132	80
				2,500	1,438	508	151	80
				5,000	1,713	601	179	80
6D	1	0.00183	0.00133	1,200	988	523	133	80
				2,500	1,538	814	149	80
				5,000	1,610	847	177	80
				7,000	1,660	874	198	80
6E	3/4	0.00258	0.00187	1,000	488	343	128	40
				2,500	838	582	139	40
				5,000	888	625	158	40

TABLE II.- EXPERIMENTAL CONDITIONS IN FRICTION AND OIL FLOW EXPERIMENTS

[$1\frac{3}{8}$-in.-diam. steel journal and bronze bearing; SAE 10 oil supplied through a 1/8-in.-diam. oil hole opposite central load]

Shaft	l/d	c_d, in.	$\frac{c_d}{d}$	Speed, N, rpm	Maximum load, P, lb	Maximum unit load, p, lb/sq in.	Maximum bearing temp., T_4, °F	Oil inlet pressure, p_o, lb/sq in.	Oil flow, Q, lb/min
6A	2	0.00252	0.00183	1,200	1,288	338	136	80	0.128
				1,200	1,288	338	135	40	.088
				1,200	1,288	338	133	120	.155
				500	938	248	130	80	.104
				500	938	248	132	120	.148
				5,000	1,663	438	169	120	.285
6B	2	0.00376	0.00273	500	836	220	129	80	0.352
				1,200	1,138	299	136	80	.412
				5,000	1,663	438	160	80	.648
				5,000	1,663	438	158	120	.786
6C	$1\frac{1}{2}$	0.00196	0.00142	1,200	938	329	132	40	0.045
				1,200	938	329	133	80	.060
				1,200	938	329	134	160	.094
				5,000	1,688	594	181	80	.132
				5,000	1,688	594	179	160	.175

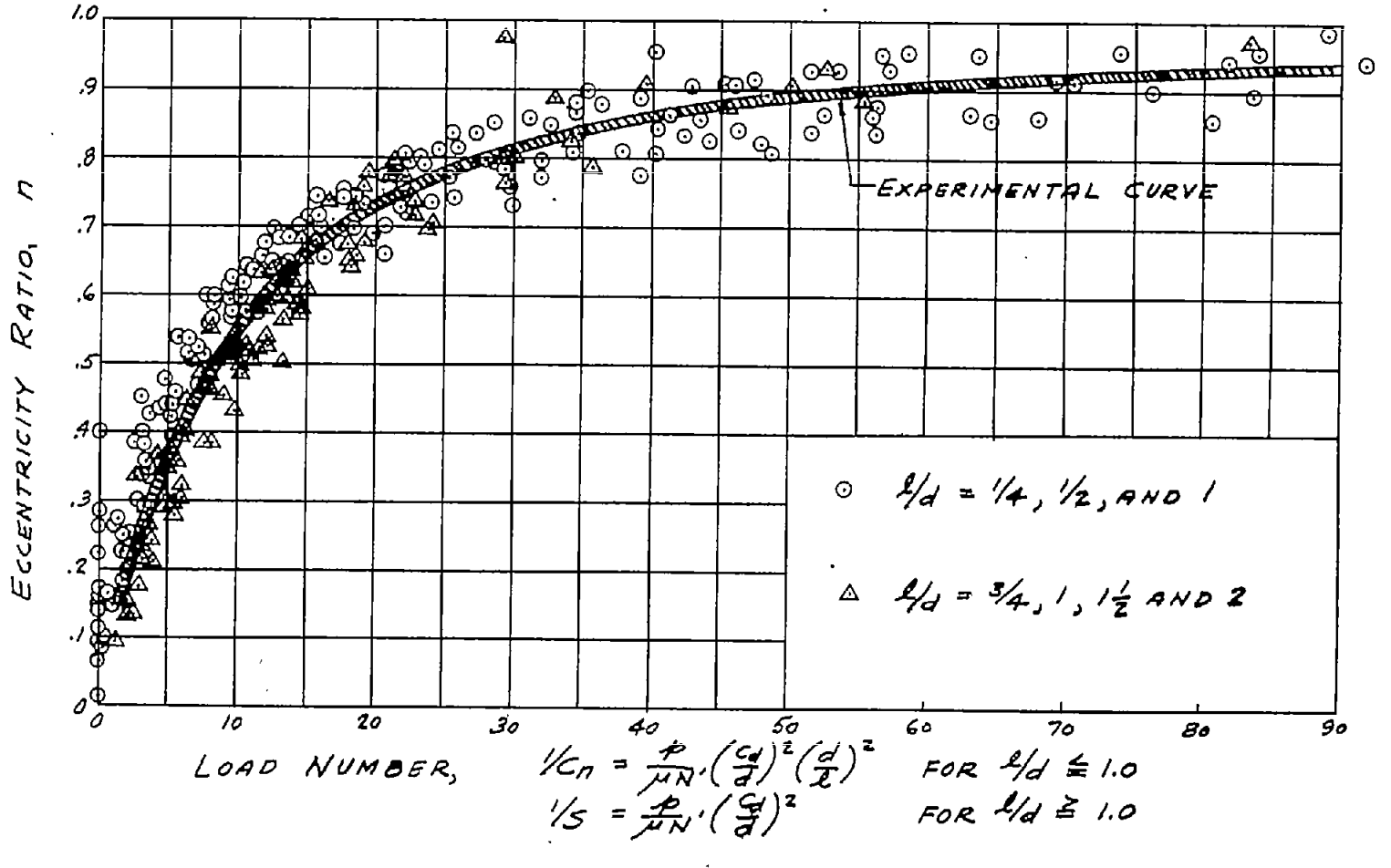

(a) Data for both long and short bearings; $l/d = 1/4, 1/2, 3/4, 1, 1\frac{1}{2}$, and 2. Data are combined from data in figures 1(b) and 1(c).

Figure 1.- Eccentricity ratio against load number.

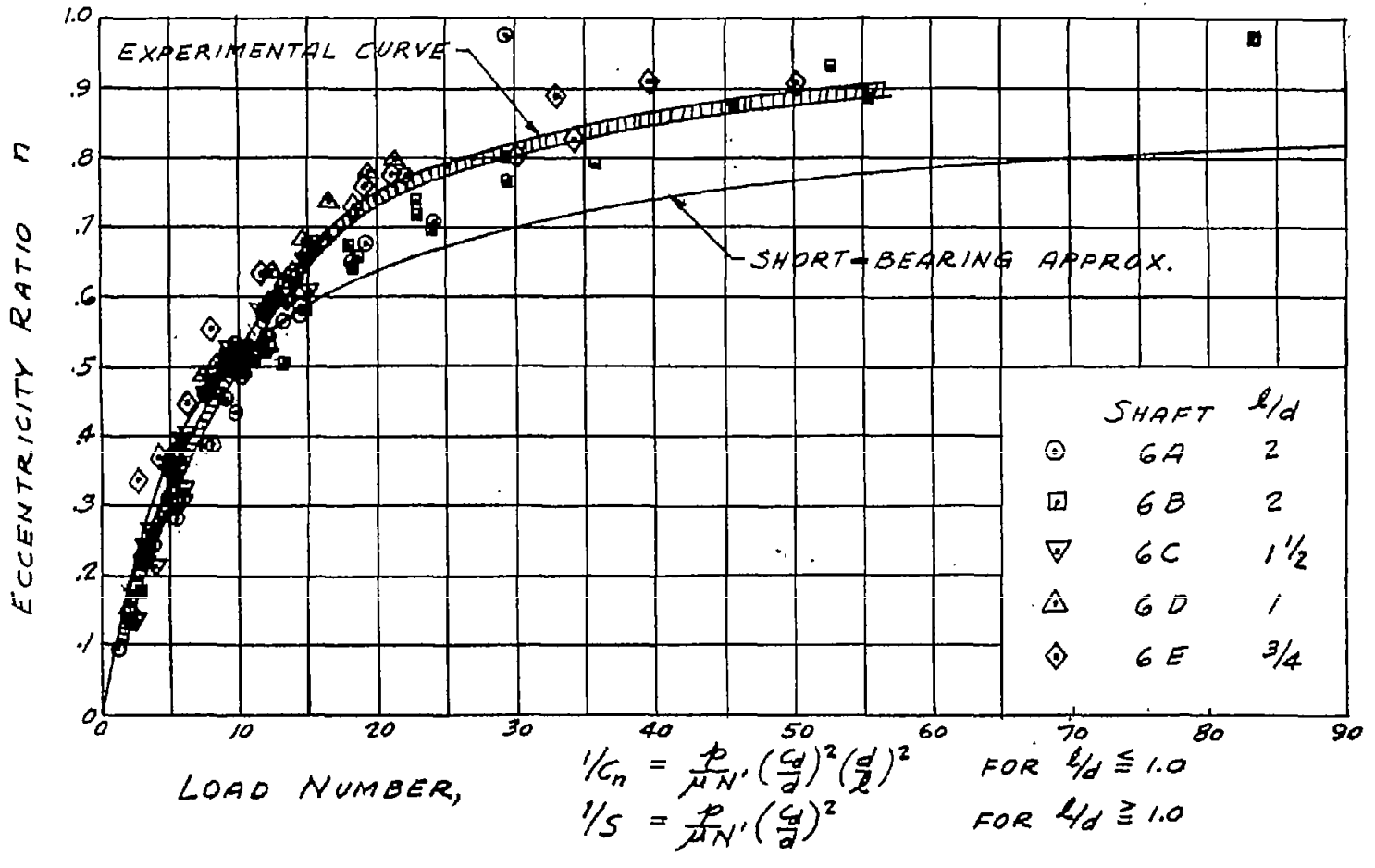

(b) Data for long bearings with $l/d = 1$, $1\frac{1}{2}$, and 2 and short bearings with $l/d = 3/4$. See table I for experimental conditions.

Figure 1.- Continued.

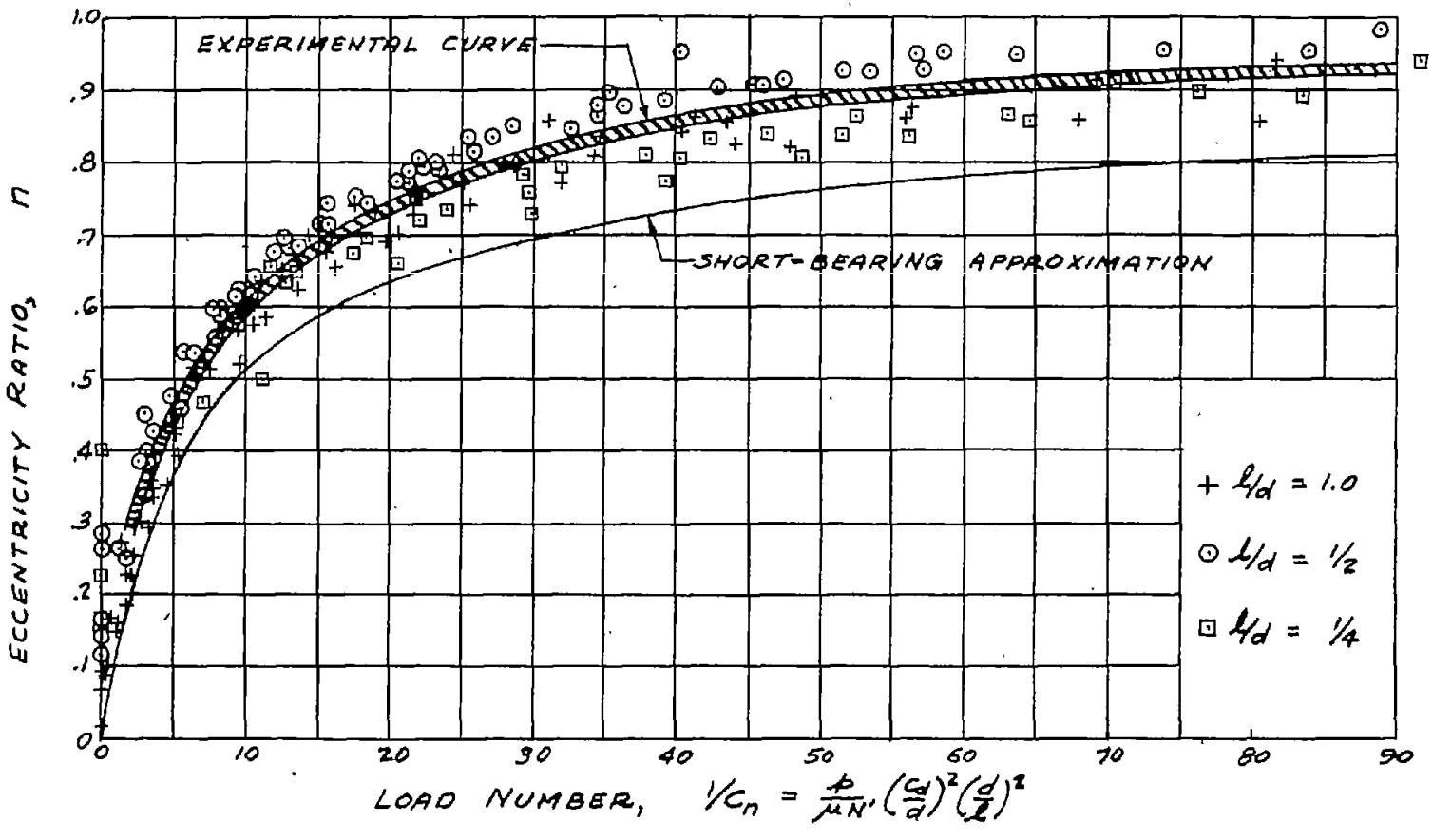

(c) Data for short bearings with $l/d = 1/4$, $1/2$, and 1. Experimental data are taken from reference 1.

Figure 1.- Concluded.

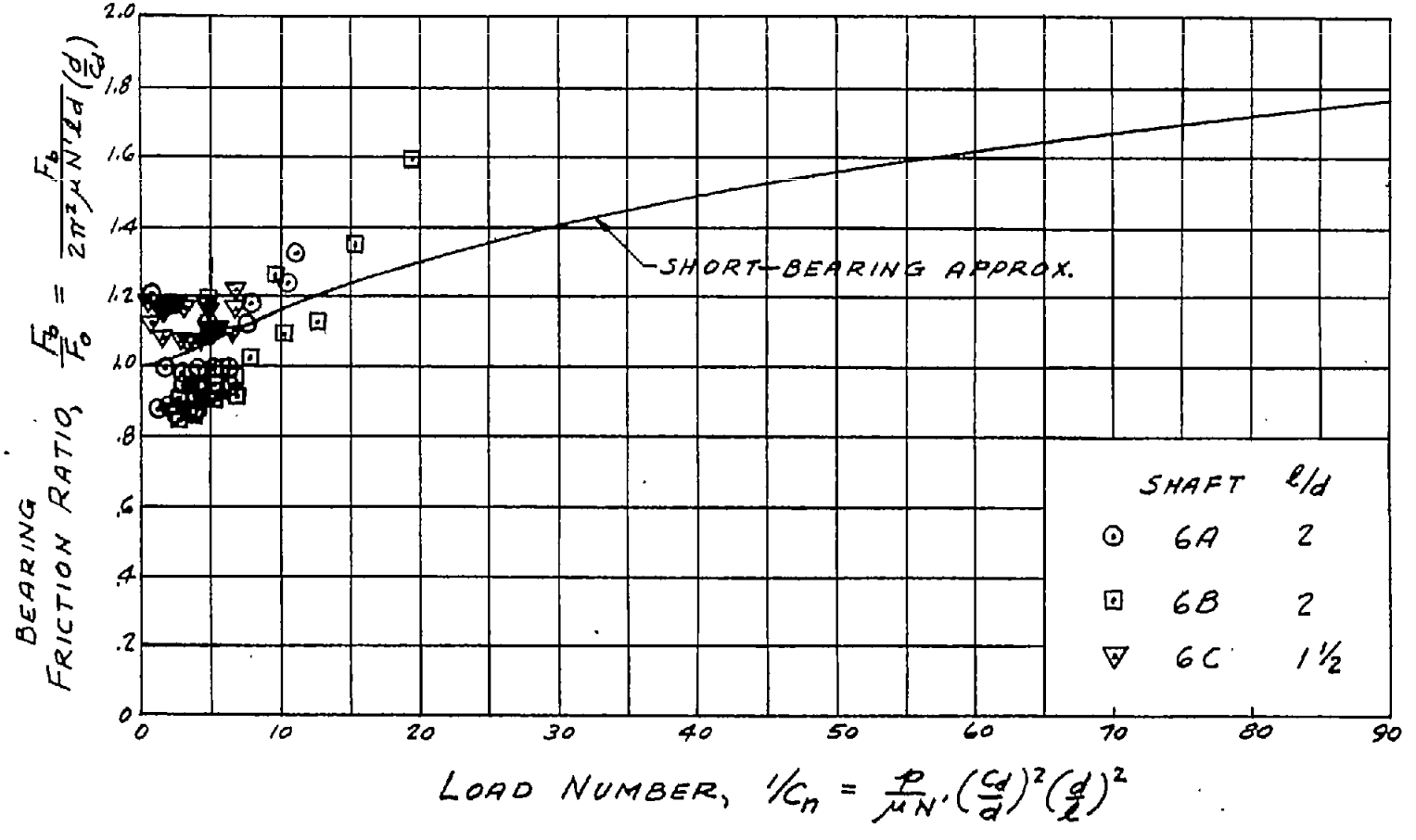

(a) Data for long bearings with $l/d = 1\frac{1}{2}$ and 2. See table II for experimental conditions.

Figure 2.- Bearing friction ratio against load number.

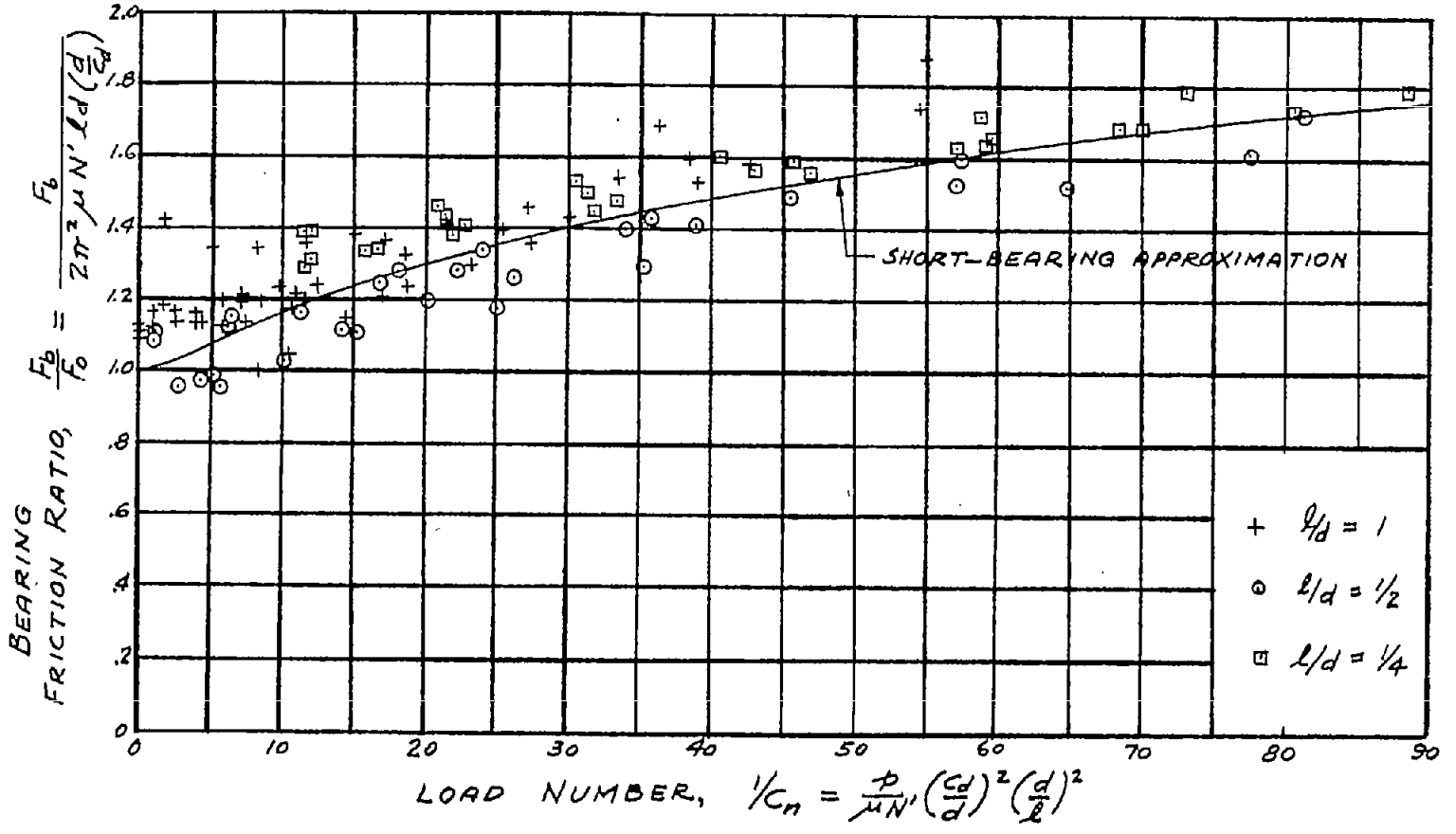

(b) Data for short bearings with $l/d = 1/4$, $1/2$, and 1. Experimental data are taken from reference 1.

Figure 2.- Concluded.

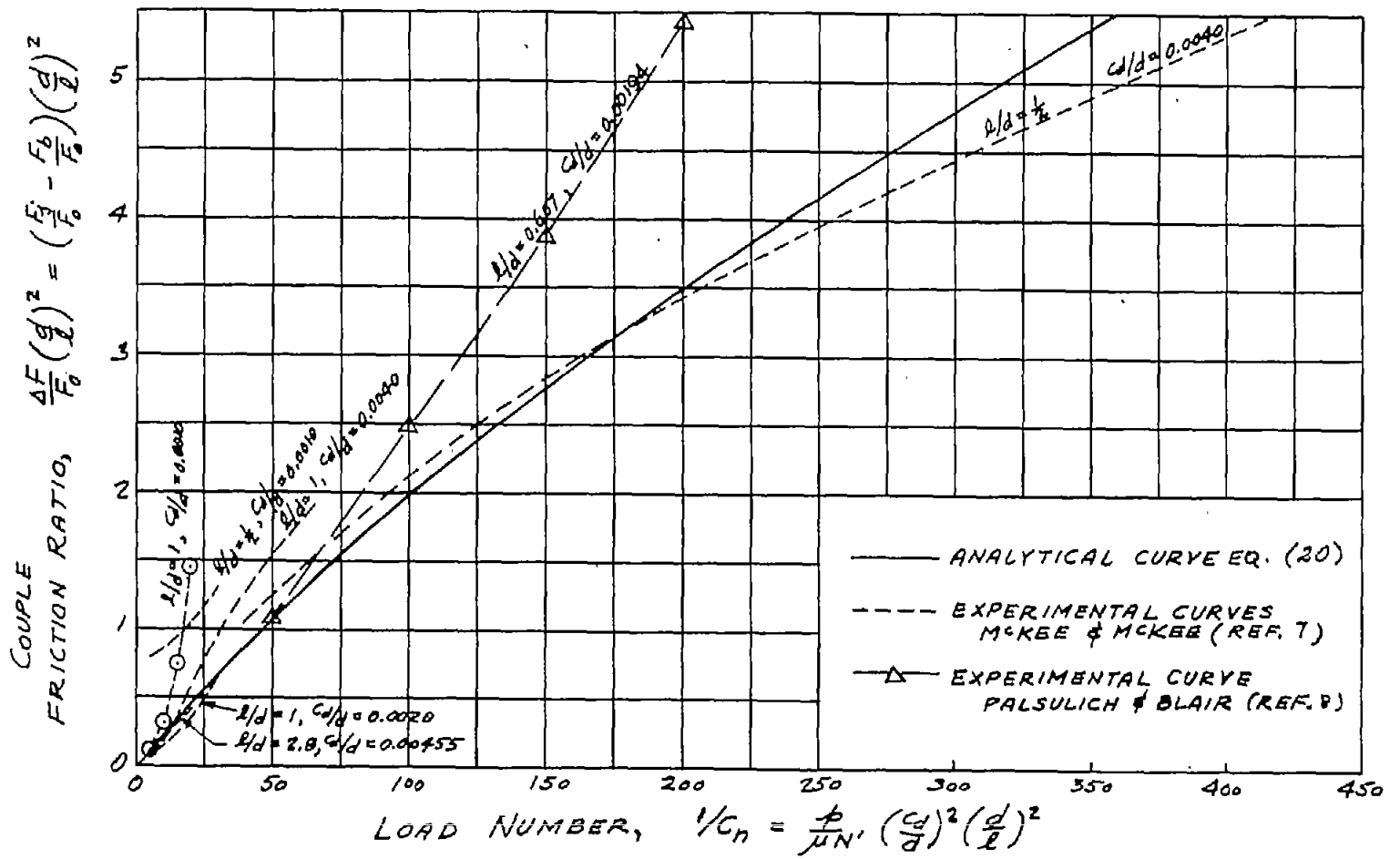

Figure 3.- Couple friction ratio against load number.

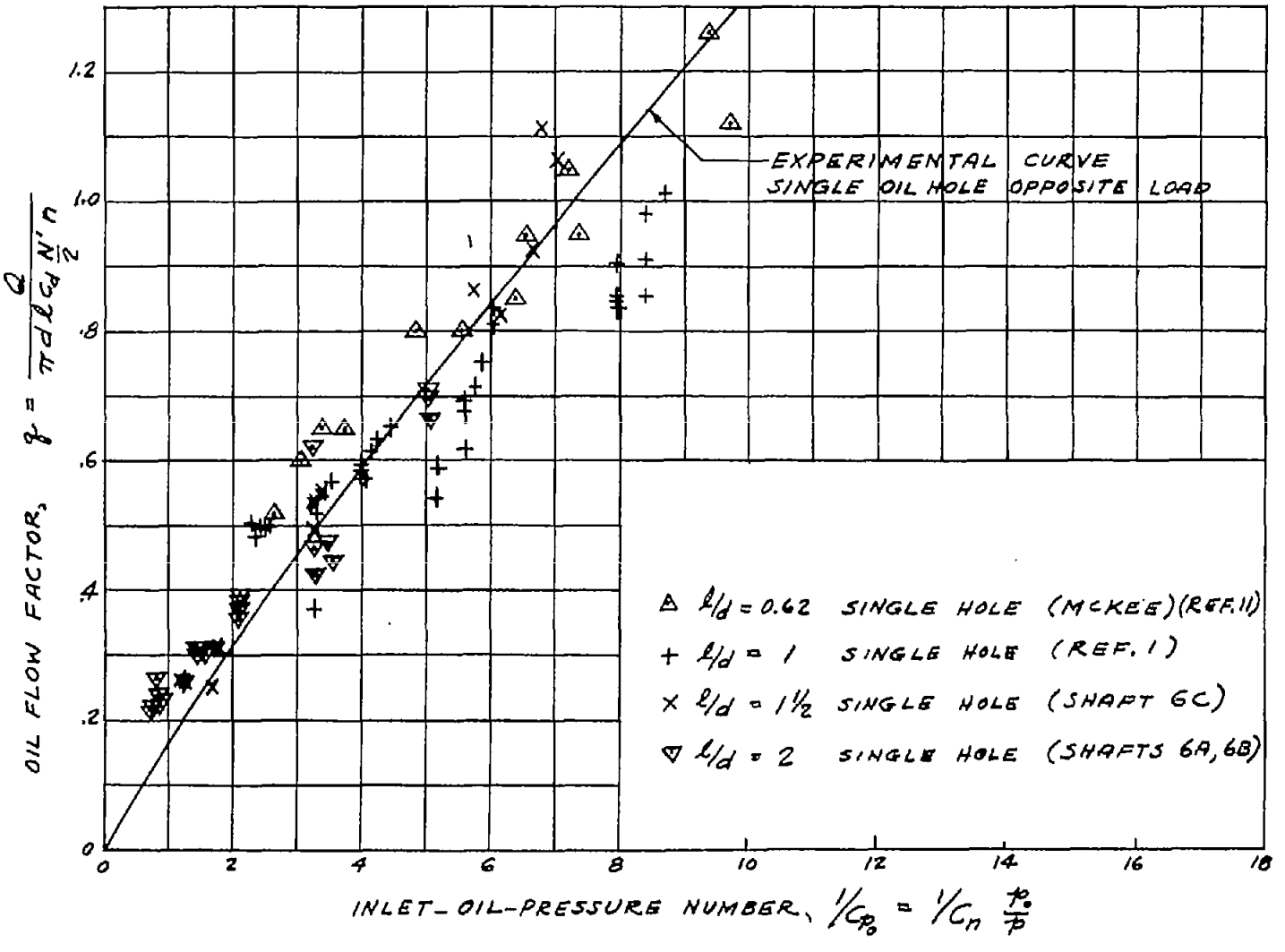

(a) Data for long bearings. See table II for experimental conditions of shafts 6A, 6B, and 6C.

Figure 4.- Oil flow factor against inlet-oil-pressure number.

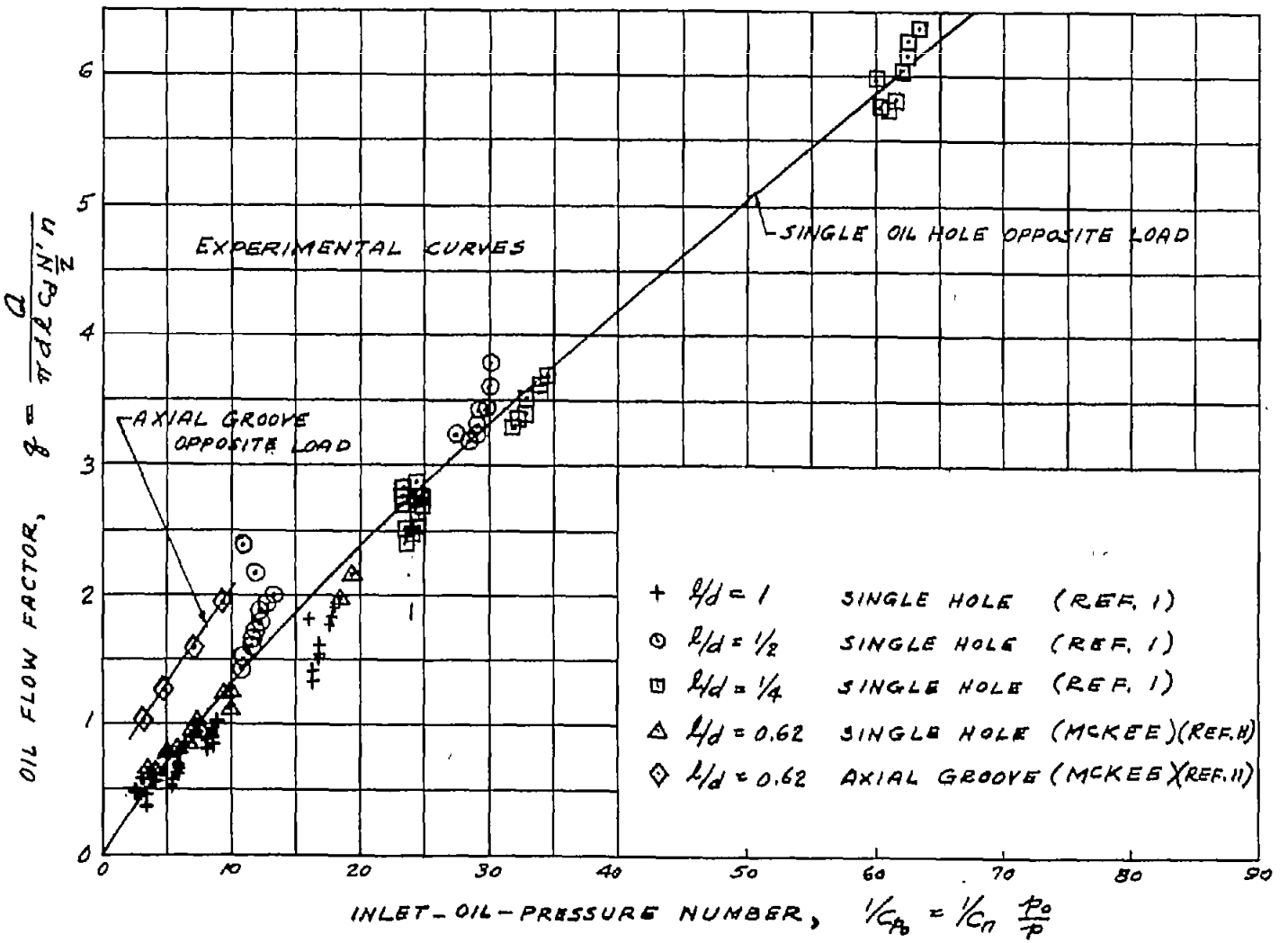

(b) Data for short bearings.

Figure 4.- Concluded.

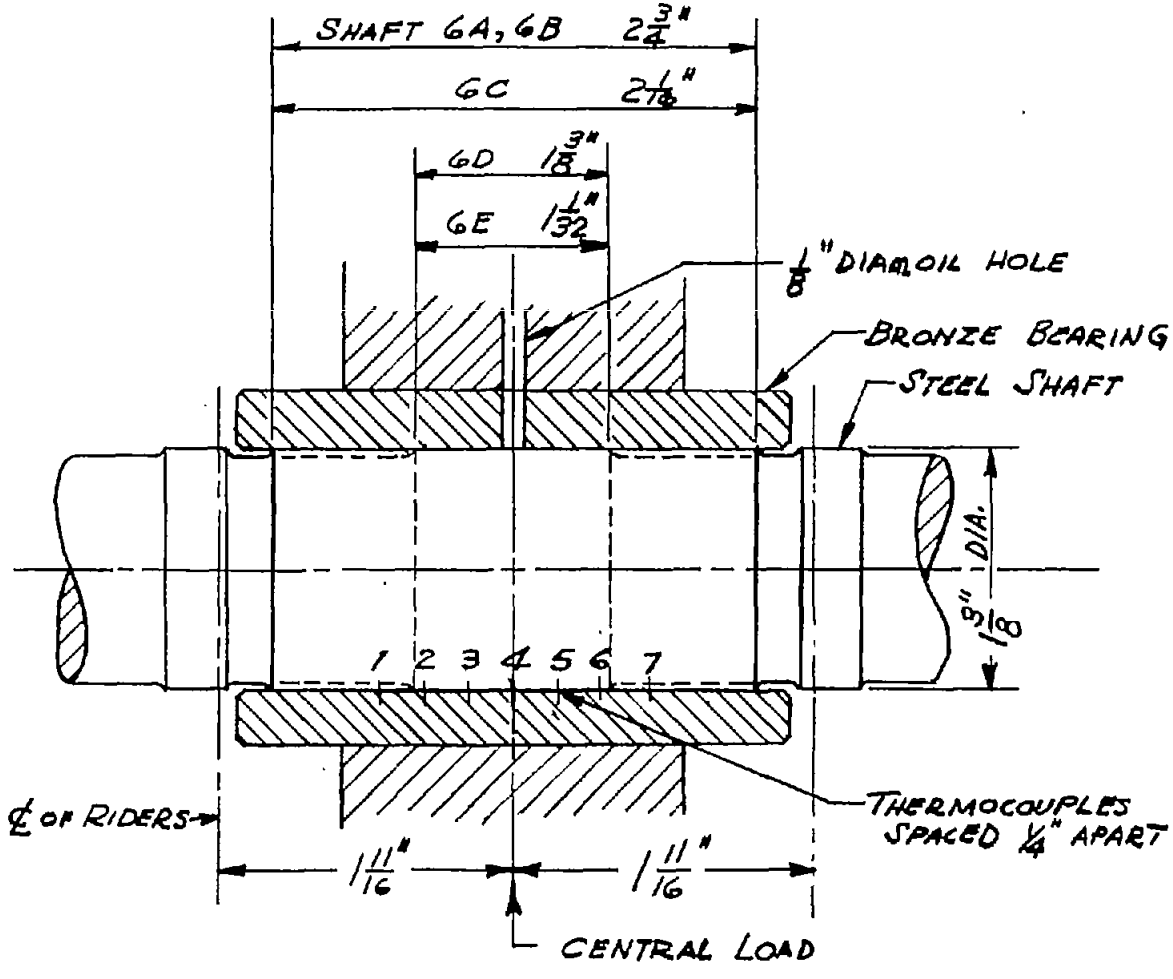

Figure 5.- Configuration of test bearing and shaft showing location of oil hole, thermocouples, and displacement-measuring riders.

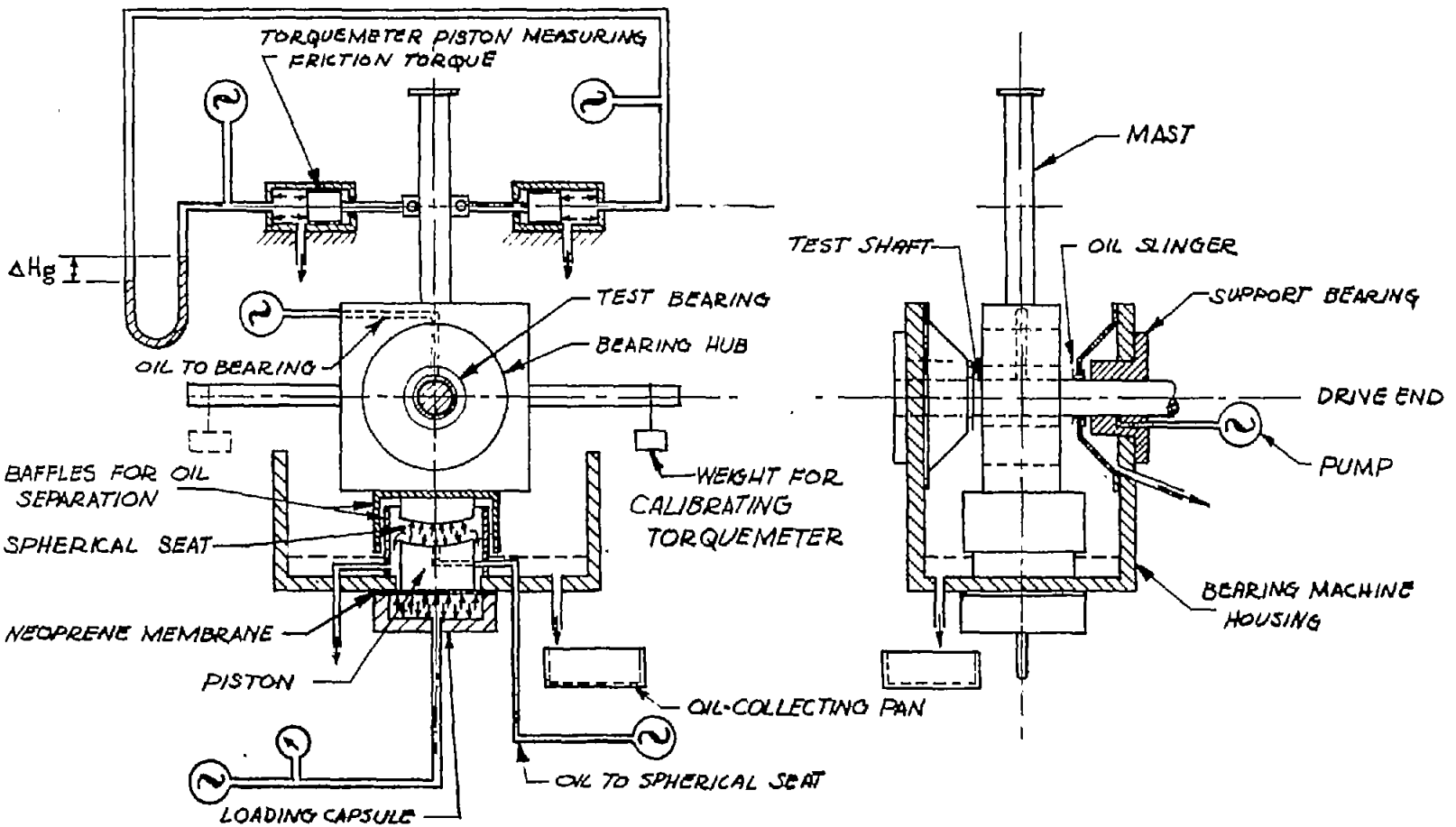

Figure 6.- Schematic diagram of apparatus for applying central load, for measuring friction torque on test bearing, and for measuring oil flow through test bearing.

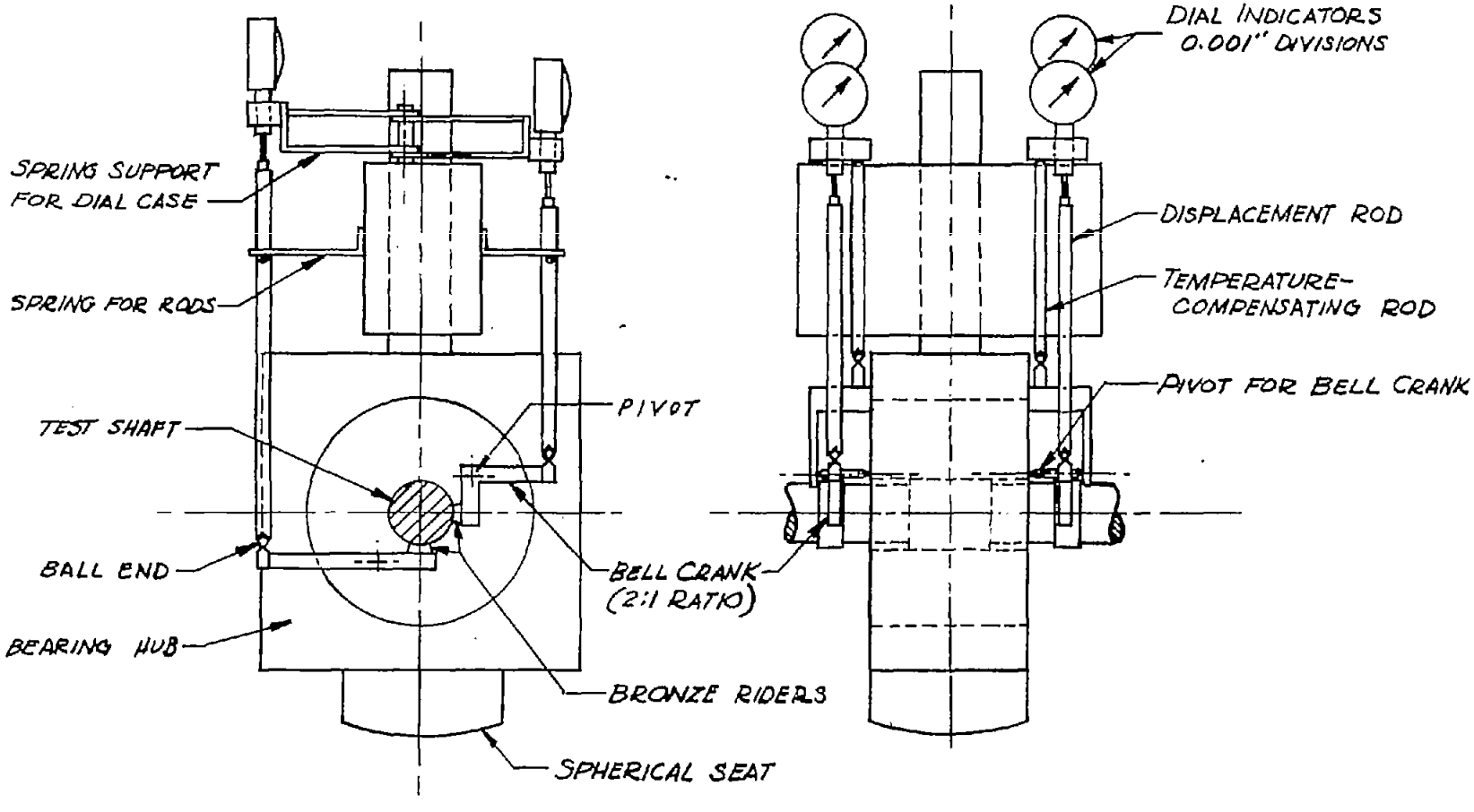

Figure 7.- Mechanical system for measuring displacement of journal relative to bearing.

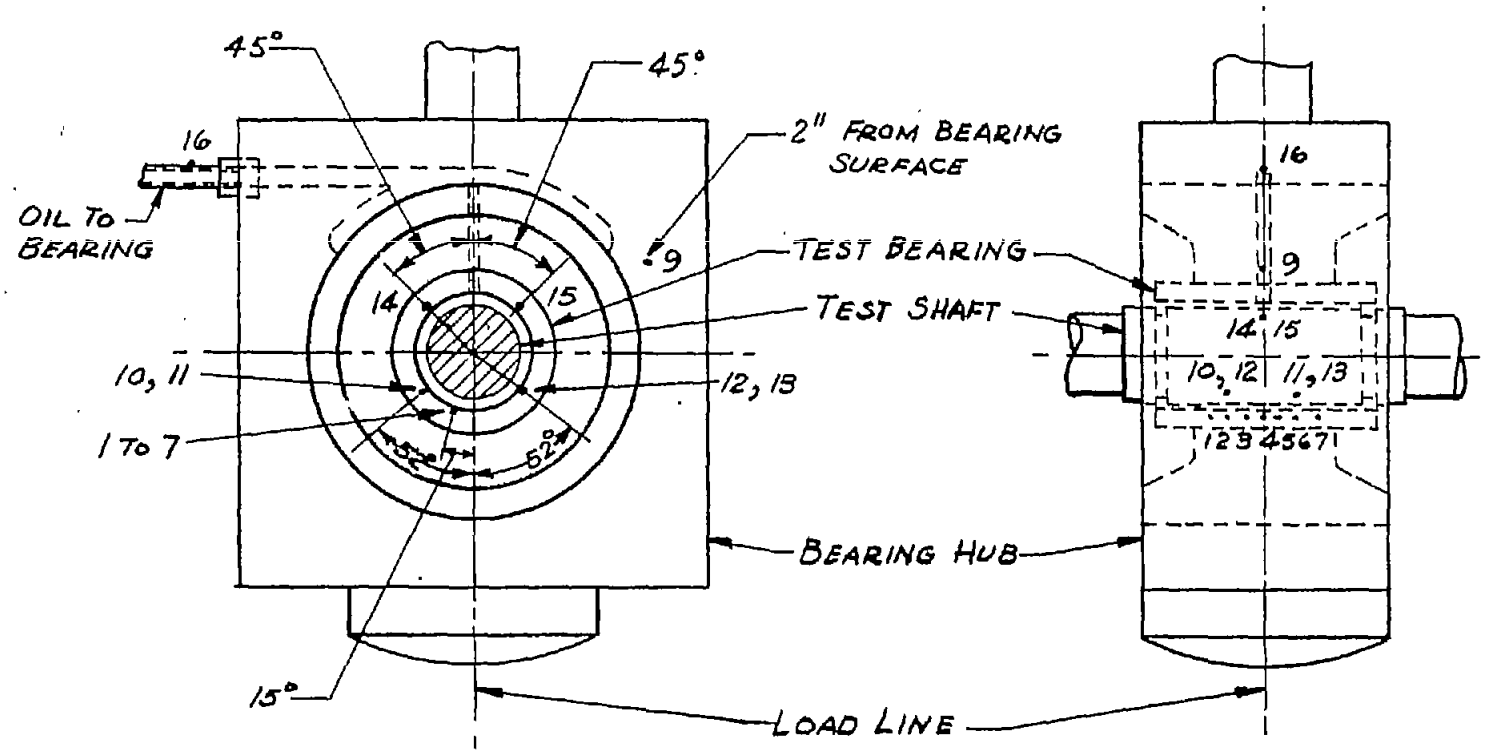

Figure 8.- Diagram of thermocouple locations. All thermocouples except 9 and 16 are located 1/16 inch from bearing surface.

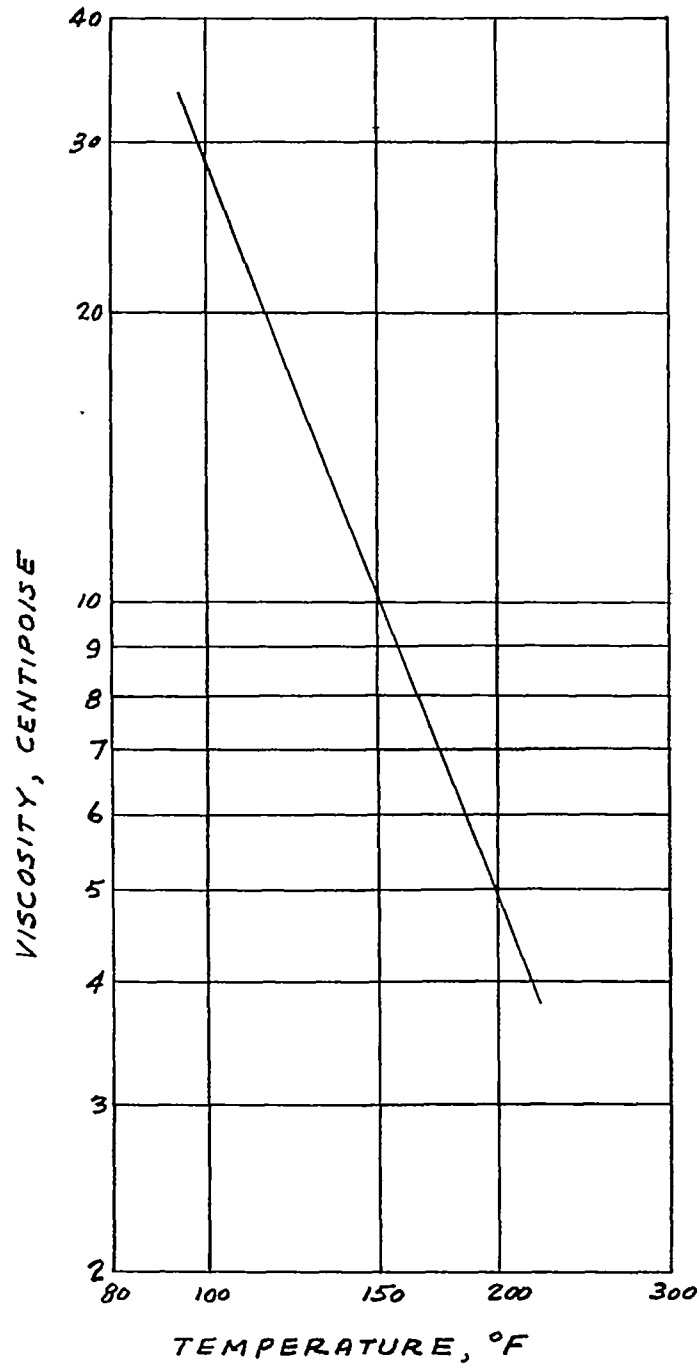

Figure 9.- Viscosity-temperature characteristics of SAE 10 oil used in experiments. Measurements of viscosity were made in a standard Saybolt viscosimeter.

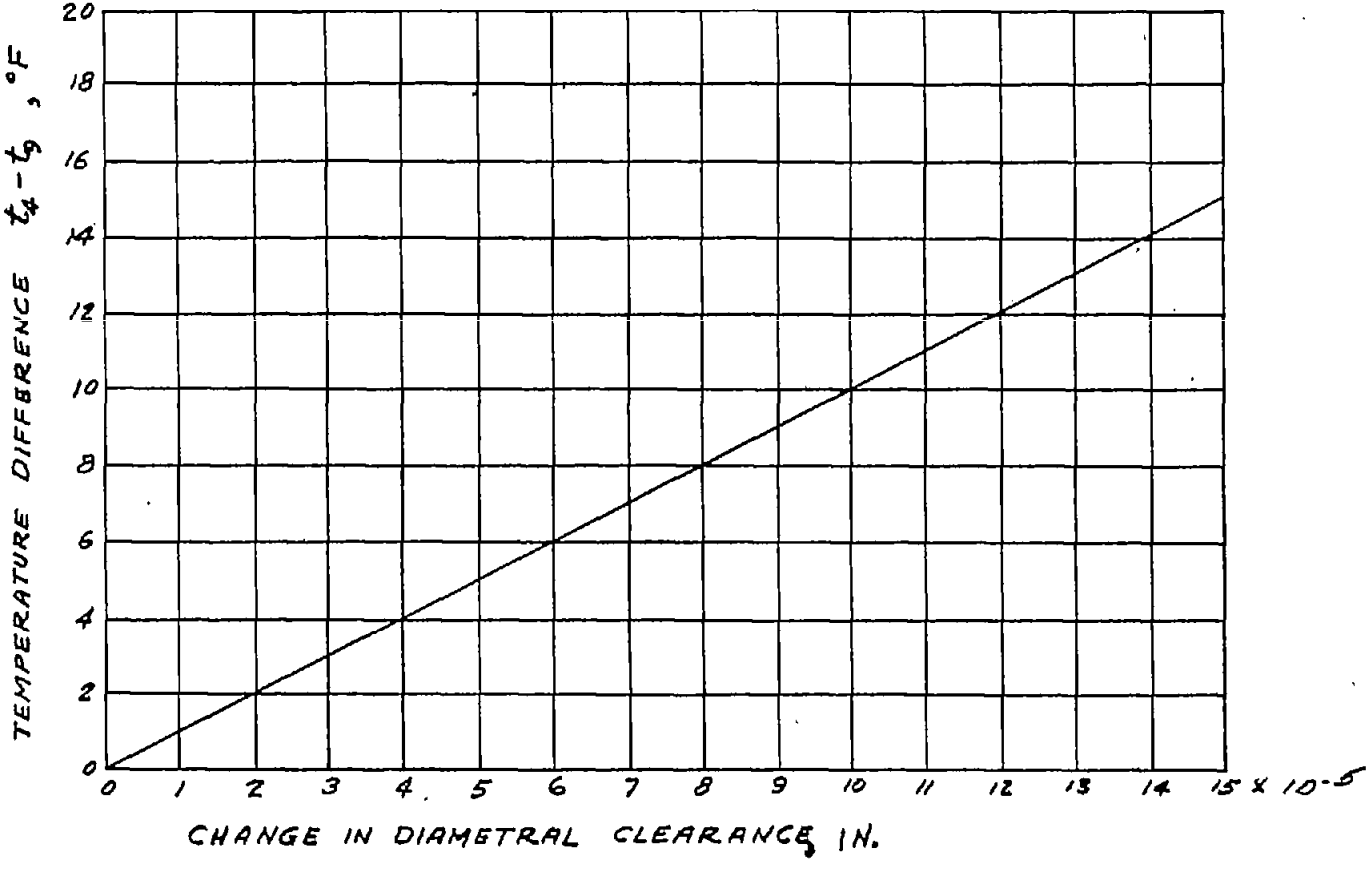

Figure 10.- Changes in diametral clearance as a function of temperature difference of two points in test-bearing wall. t_4 and t_9 are bearing temperatures at 1/16 inch and 2 inches, respectively, from bearing surface. Running clearances of test bearing are determined by subtracting change in clearance from room-temperature clearance.

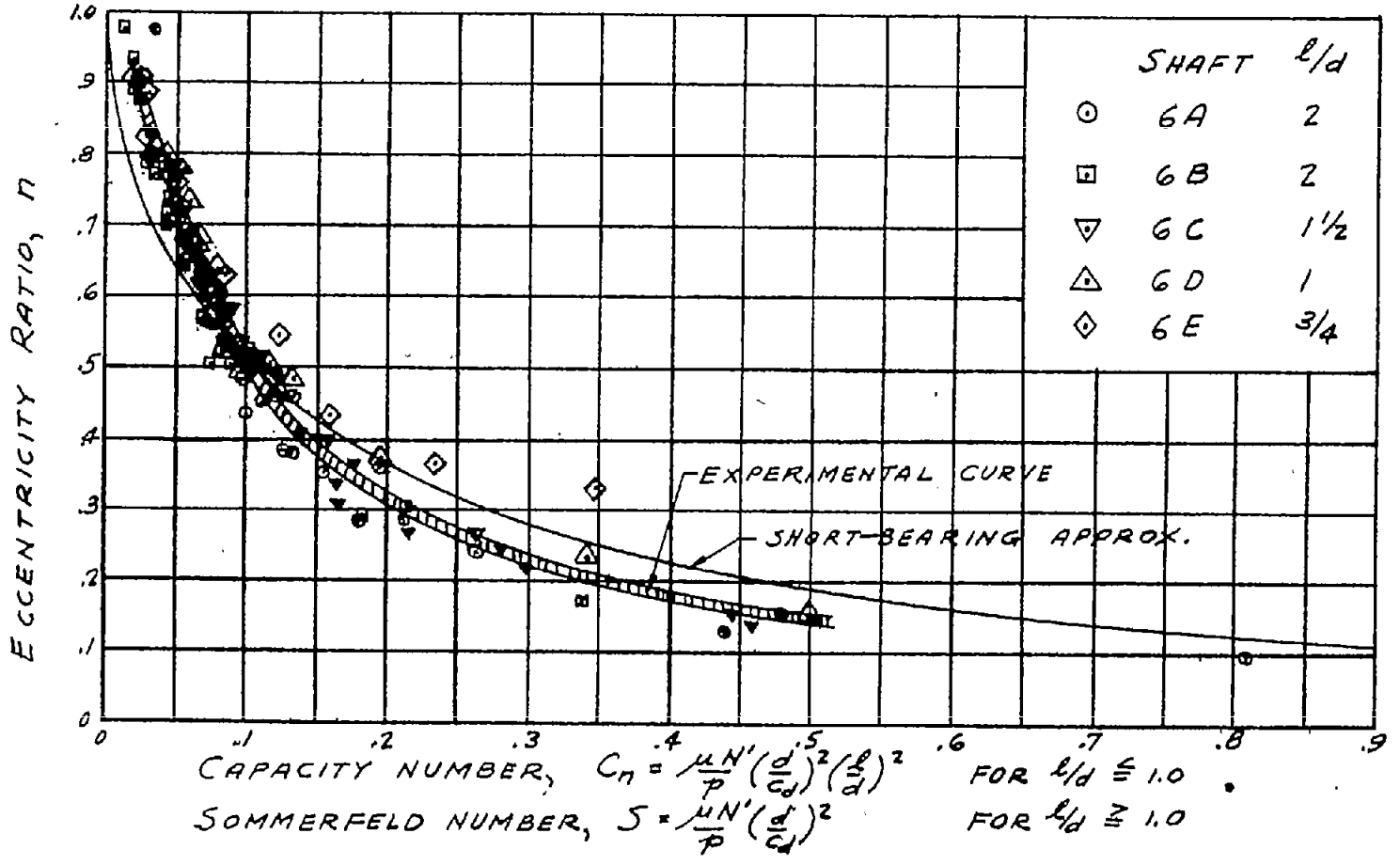

(a) Long bearings with $l/d = 1, 1\frac{1}{2}$, and 2 and short bearings with $l/d = 3/4$. Experimental data are same as in figure 1(b); for experimental conditions, see table I.

Figure 11.- Eccentricity ratio against Sommerfeld number and capacity number.

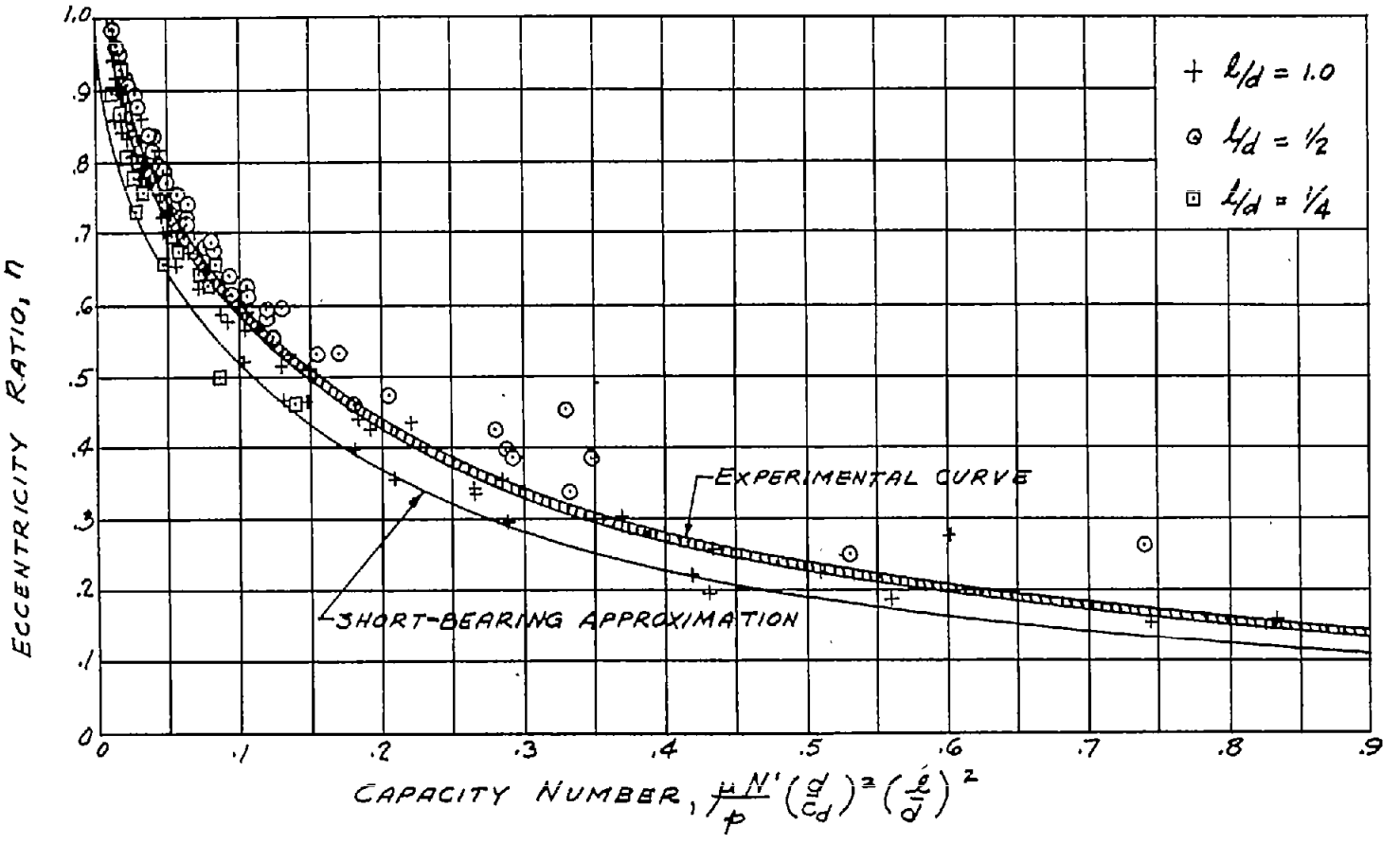

(b) Short bearings with $l/d = 1/4$, $1/2$, and 1. Experimental data are same as in figure 1(c) and are from reference 1.

Figure 11.- Concluded.

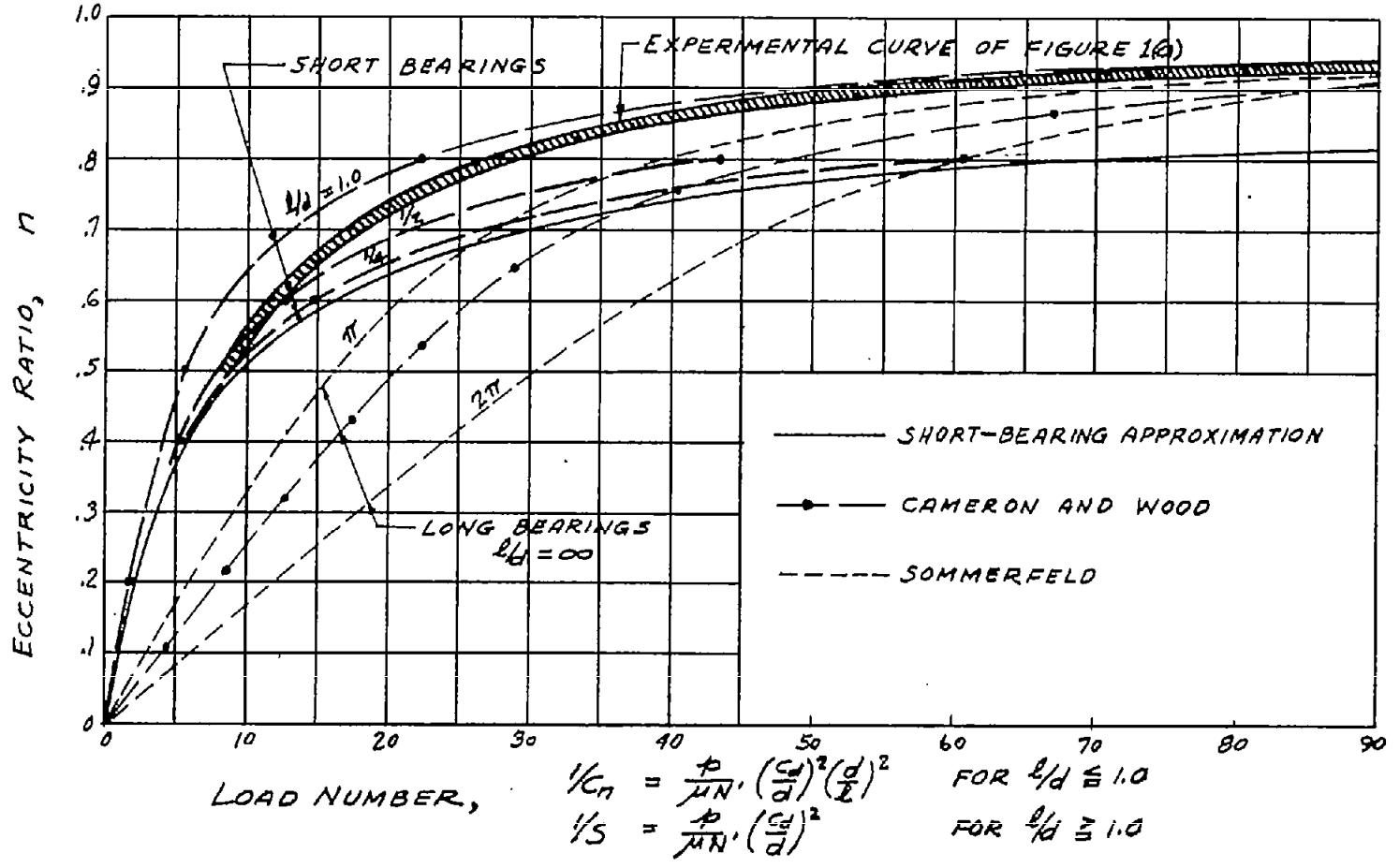

Figure 12.- Analytical curves of eccentricity ratio against load number.

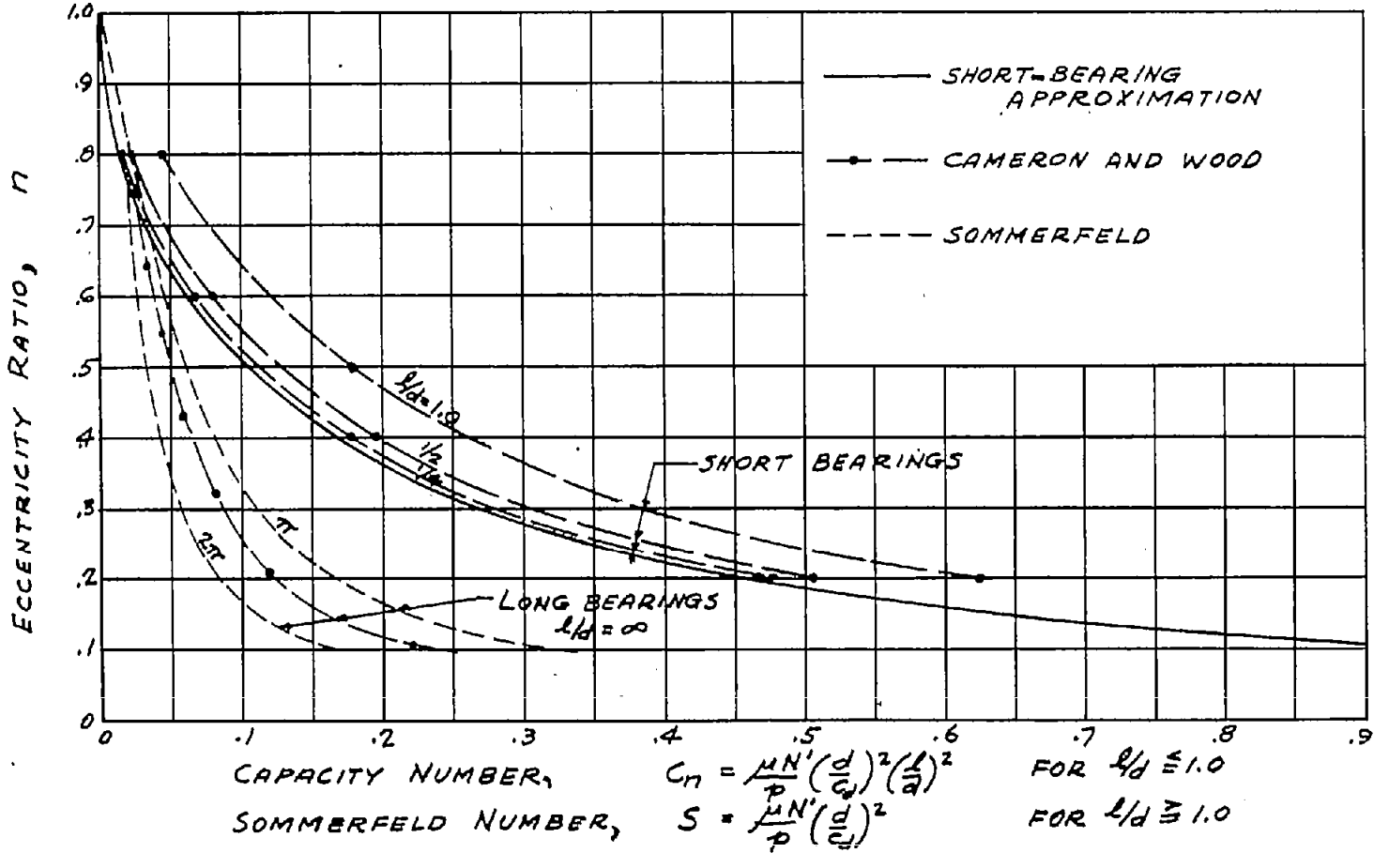

Figure 13.- Analytical curves of eccentricity ratio against Sommerfeld number and capacity number.

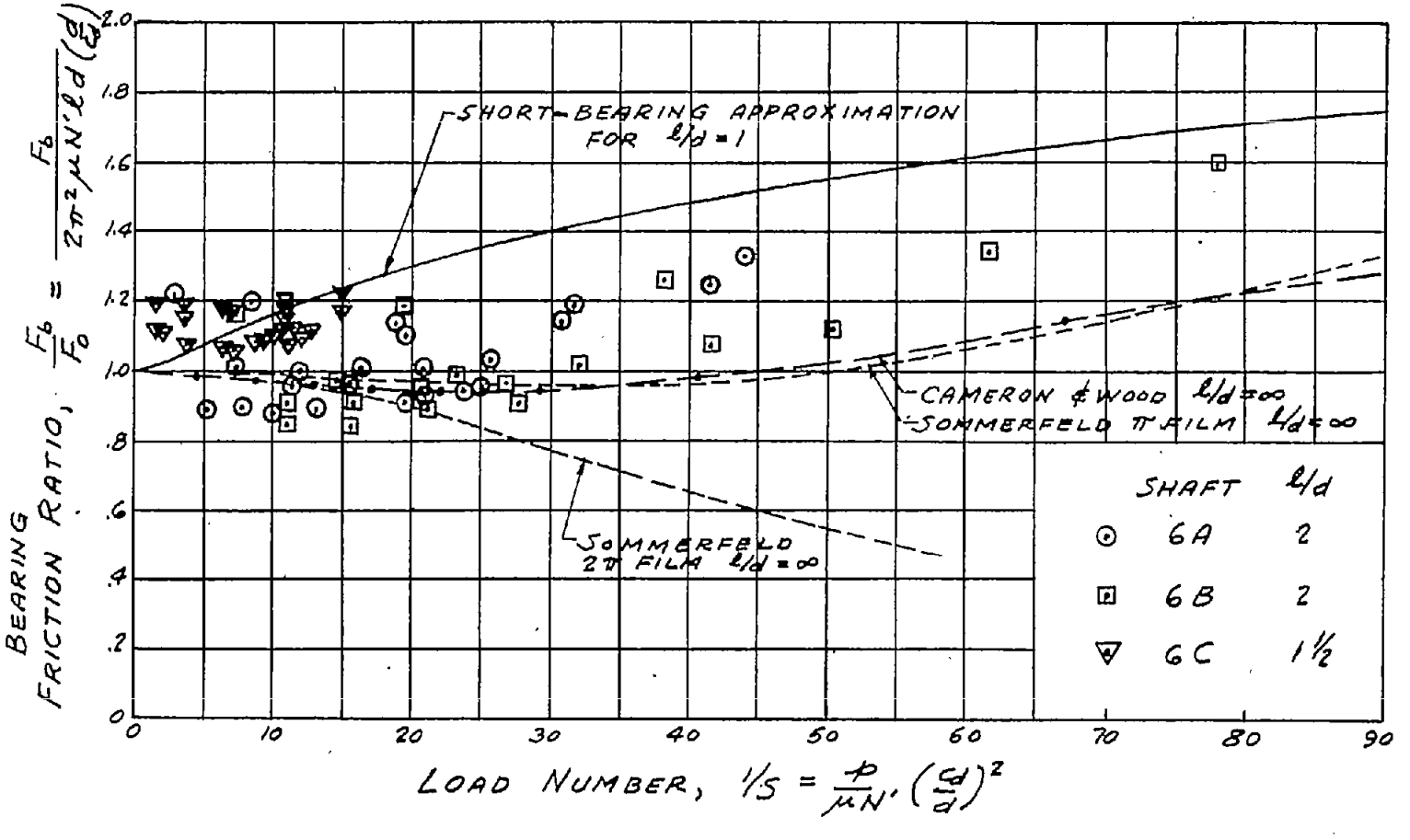

(a) Comparison of long-bearing data with analytical curves.

Figure 14.- Bearing friction ratio against load number.

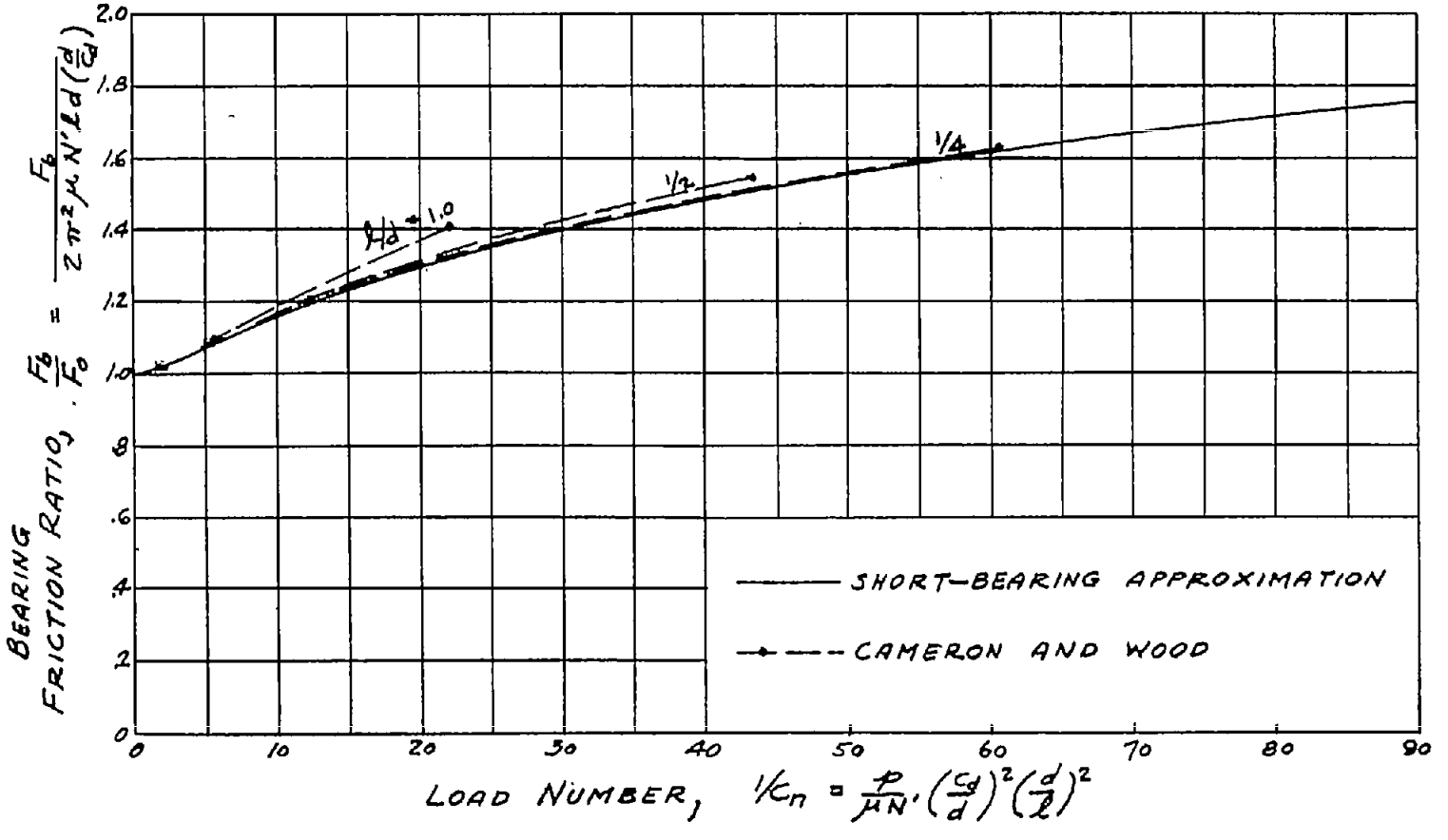

(b) Analytical curves for short bearings.

Figure 14.- Concluded.

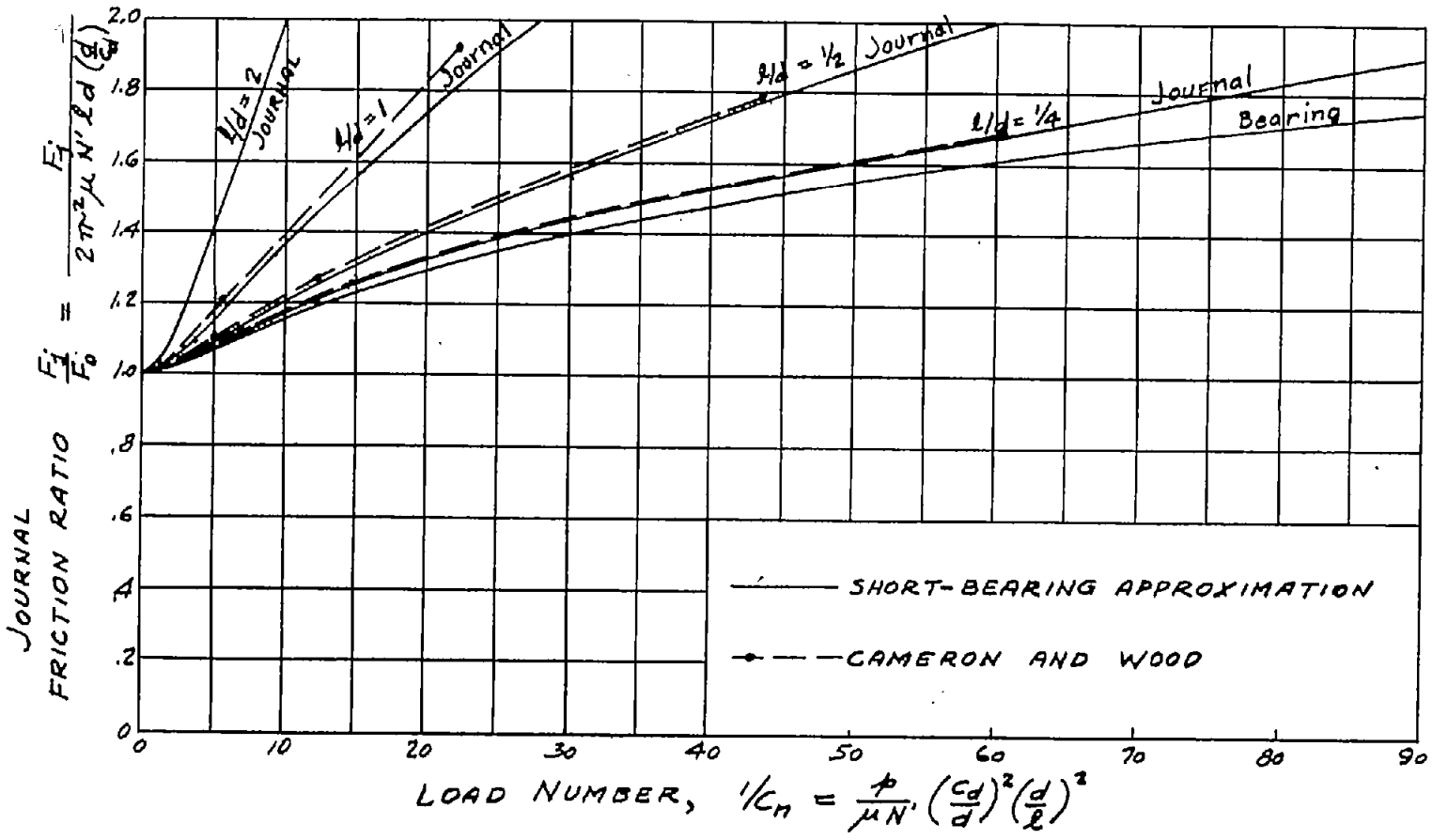

(a) Analytical curves for long and short bearings; Cameron and Wood curves taken from reference 2.

Figure 15.- Curves of journal friction ratio against load number.

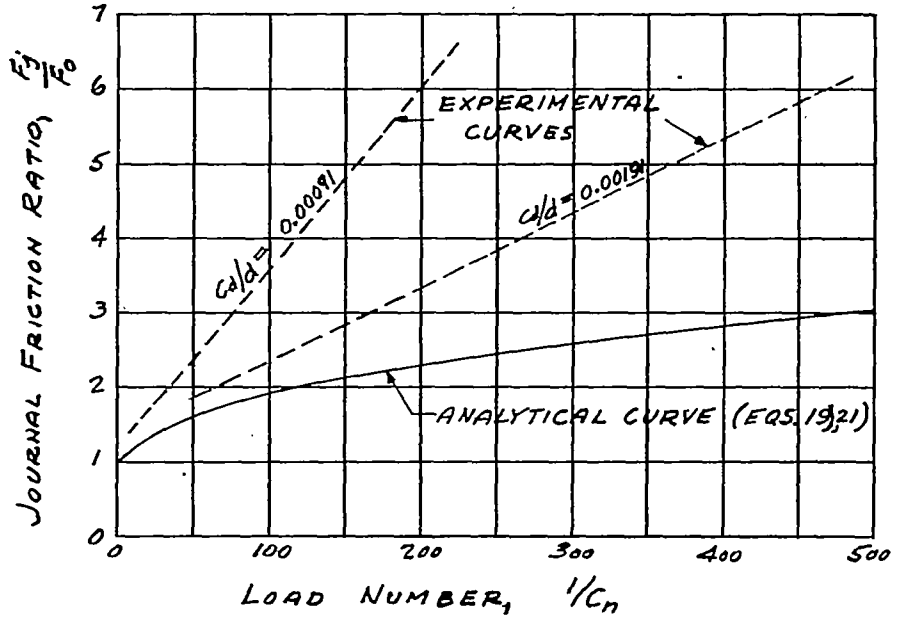

(b) Comparison of experimental curves of McKee and McKee (ref. 7) with analytical curves of equations (19) and (21); $l/d = 1/4$.

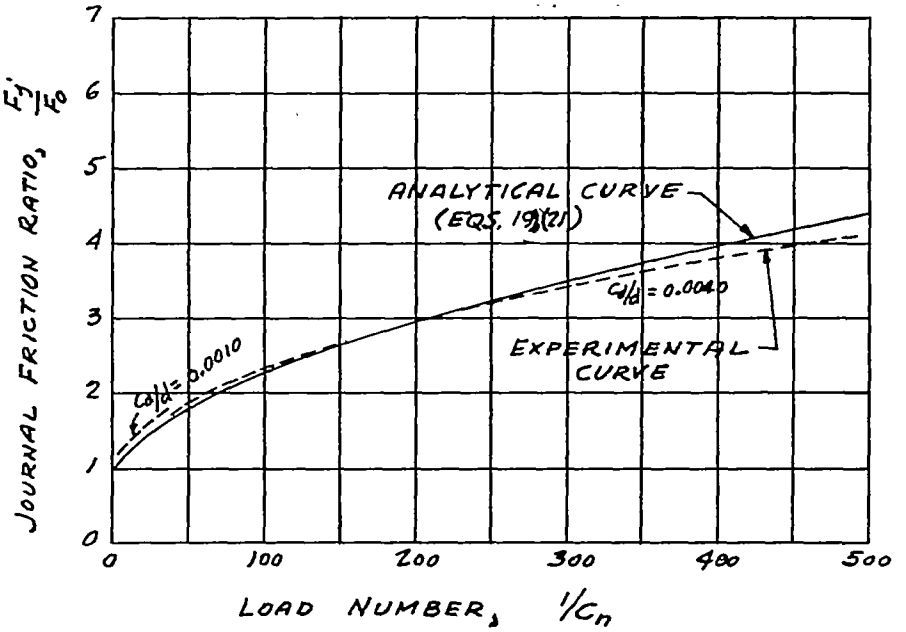

(c) Comparison of experimental curves of McKee and McKee (ref. 7) with analytical curves of equations (19) and (21); $l/d = 1/2$.

Figure 15.- Continued.

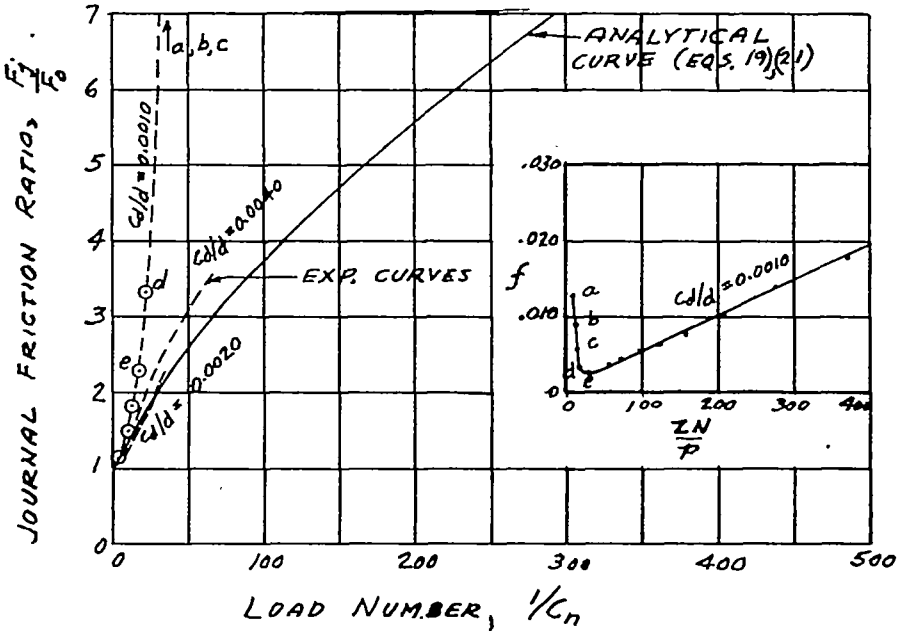

(d) Comparison of experimental curves of McKee and McKee (ref. 7) with analytical curves of equations (19) and (21); $l/d = 1$.

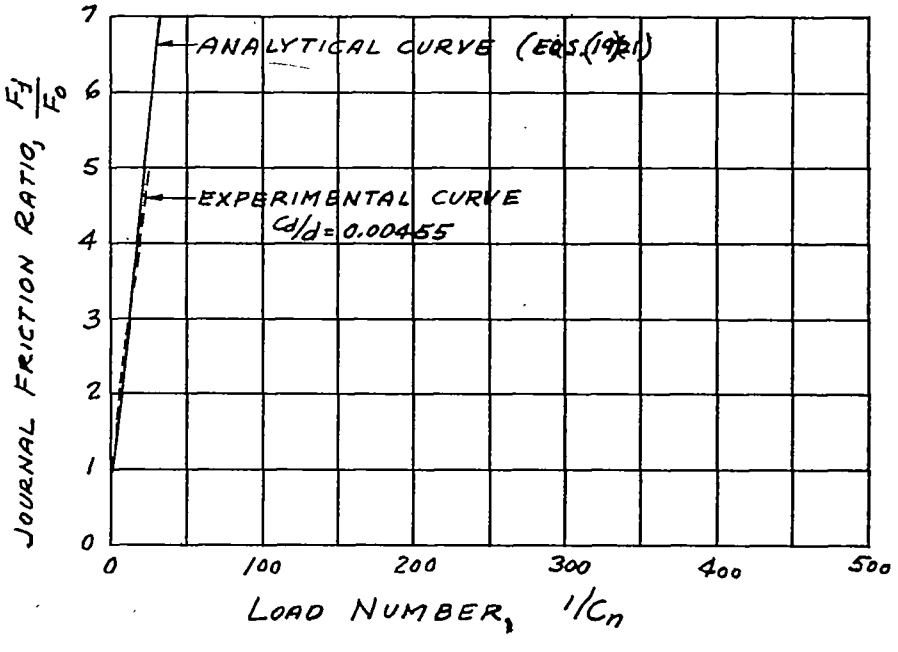

(e) Comparison of experimental curves of McKee and McKee (ref. 7) with analytical curves of equations (19) and (21); $l/d = 2.8$.

Figure 15.- Continued.

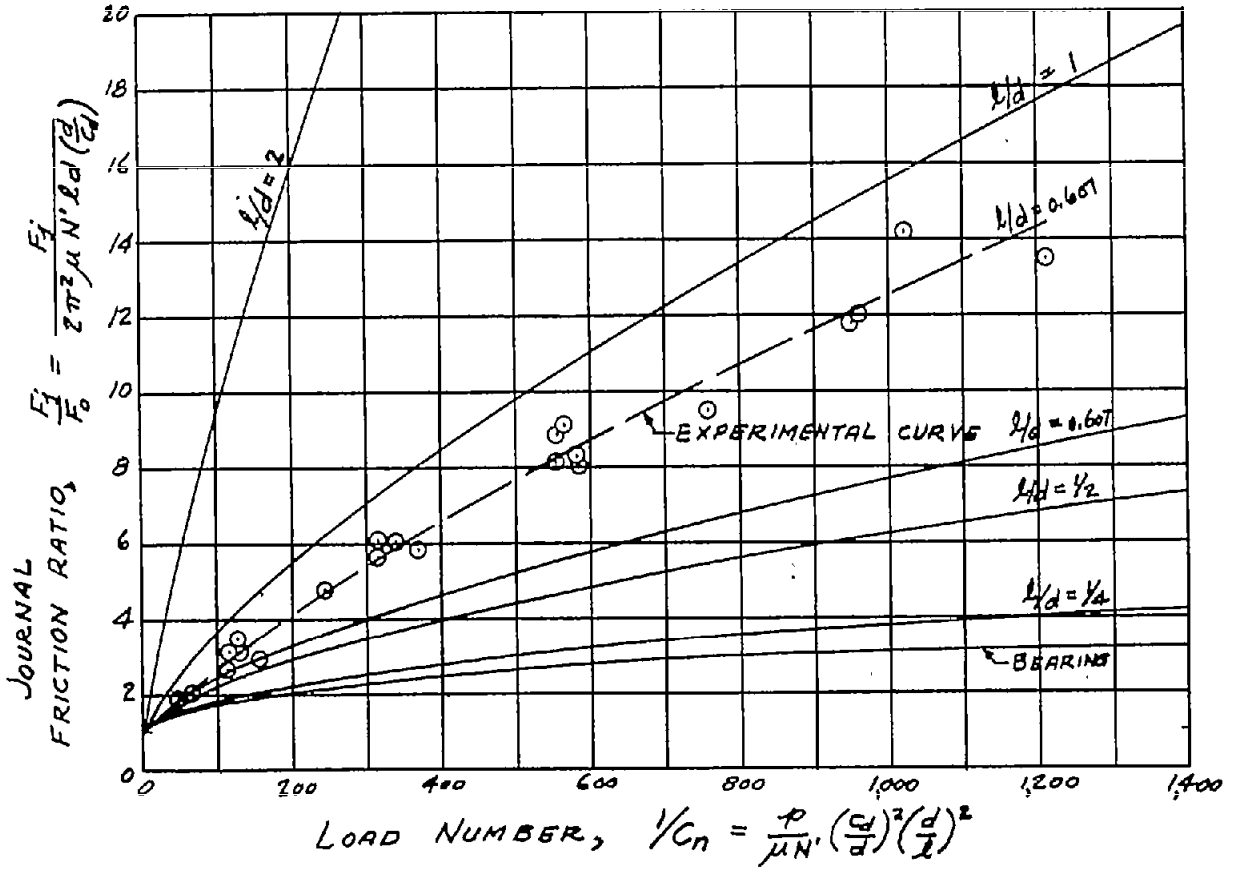

(f) Comparison of experimental data of Palsulich and Blair (ref. 8) with analytical curves of equations (19) and (21); long and short bearings.

Figure 15.- Concluded.

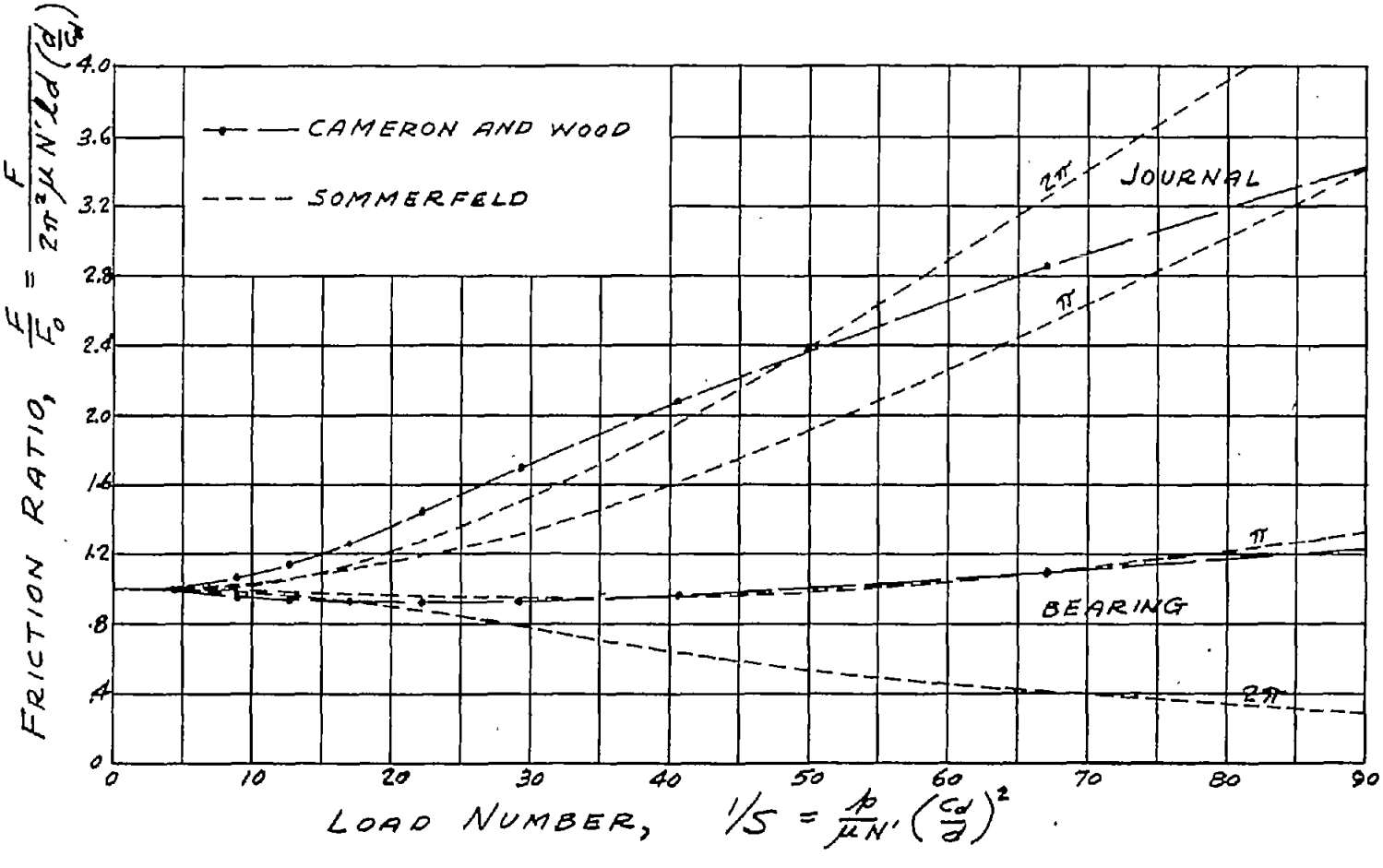

Figure 16.- Analytical curves of journal and bearing friction ratio against 1/S for infinite values of l/d.

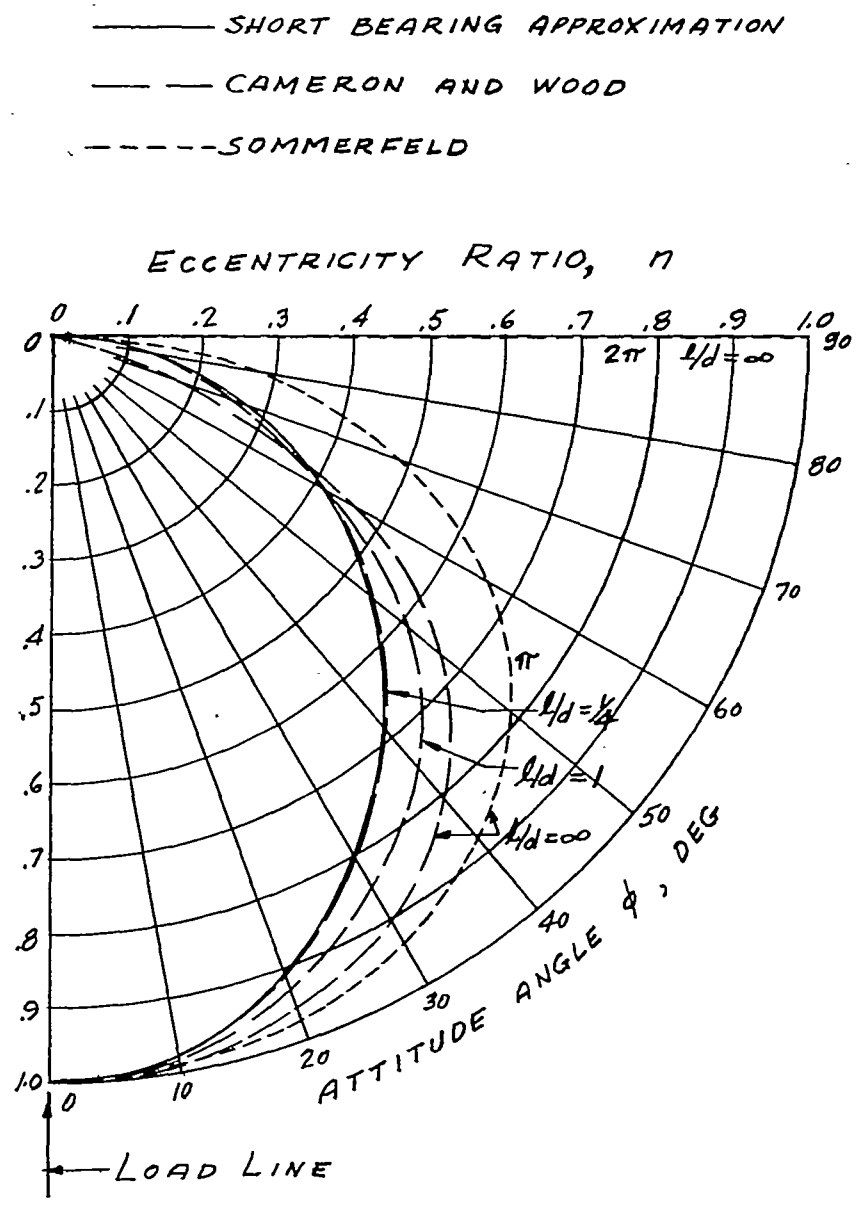

Figure 17.- Clearance circle diagram showing paths of journal displacement relative to bearing under central loading in terms of eccentricity ratio against altitude angle; analytical curves.

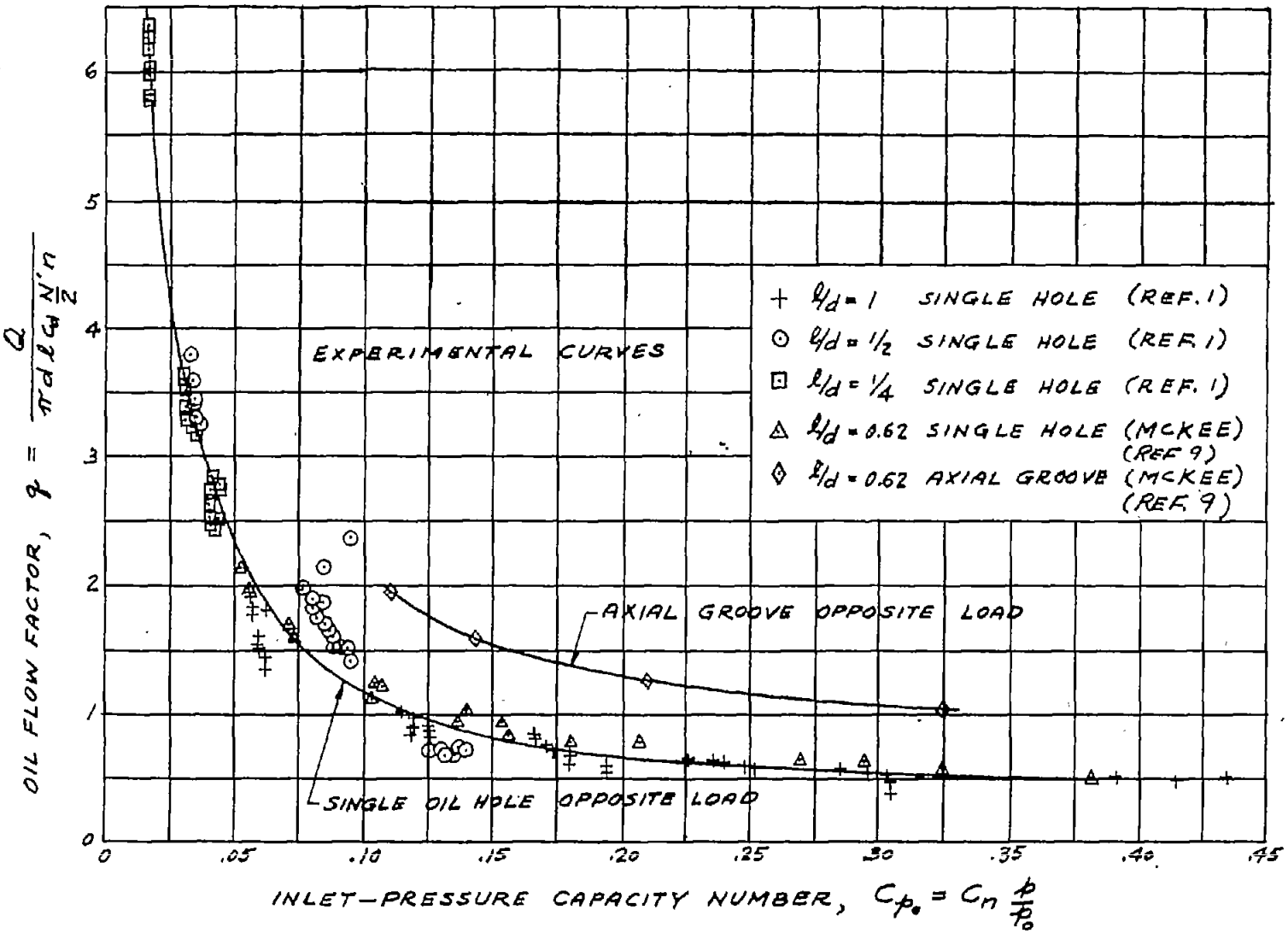

Figure 18.- Oil flow factor against inlet-pressure capacity number for short bearings with l/d = 1/4, 1/2, 0.62, and 1. Experimental data are from references 1 and 9 and are also shown in figure 4(b).